JACS
JOURNAL OF THE AMERICAN CHEMICAL SOCIETY
pubs.acs.org/JACS
Article

An Ultramicroporous Metal–Organic Framework for High Sieving Separation of Propylene from Propane

Bin Liang,[§] Xin Zhang,[§] Yi Xie, Rui-Biao Lin,* Rajamani Krishna, Hui Cui, Zhiqiang Li, Yanshu Shi, Hui Wu, Wei Zhou,* and Banglin Chen*

Cite This: J. Am. Chem. Soc. 2020, 142, 17795–17801
Read Online

ABSTRACT: Highly selective adsorptive separation of olefin/paraffin through porous materials can produce high purity olefins in a much more energy-efficient way than the traditional cryogenic distillation. Here we report an ultramicroporous cobalt gallate metal–organic framework (Co-gallate) for the highly selective sieving separation of propylene/propane at ambient conditions. This material possesses optimal pore structure for the exact confinement of propylene molecules while excluding the slightly large propane molecules, as clearly demonstrated in the neutron diffraction crystal structure of Co-gallate⊃0.38C_3D_6. Its high separation performance has been confirmed by the gas sorption isotherms and column breakthrough experiments to produce the high purity of propylene (97.7%) with a high dynamic separation productivity of 36.4 cm^3 cm^{-3} under ambient conditions. The gas adsorption measurement, pore size distribution, and crystallographic and modeling studies comprehensively support the high sieving C_3H_6/C_3H_8 separation in this MOF material. It is stable under different environments, providing its potential for the industrial propylene purification.

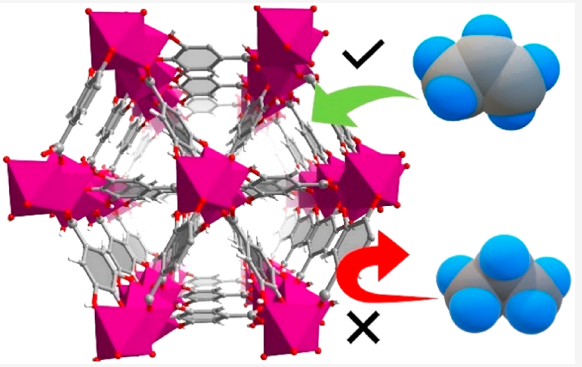

INTRODUCTION

Propylene is a prime olefin feedstock in the petrochemical industry for the manufacture of a variety of chemical commodities, including polypropylene. Due to the good resistance to fatigue, heat, and organic solvents, polypropylene has been widely used for films, fibers, containers, packaging, and especially for personal protective medical or laboratory items.[1] The worldwide production capacity of propylene was up to 114 million metric tons in 2015. It is essential to upgrade the propylene/propane mixture to high-purity propylene in order to produce polypropylene.[2,3] Compared to ethylene and ethane, propylene and propane show a higher similarity in their physical properties such as volatilities. Specifically, the boiling point difference of propylene/propane is about 5 K, much smaller than that of ethylene/ethane (15 K). The established method for propylene/propane separation involves repeated distillation–compression cycling in giant C3 splitter towers of up to 300 feet high with over 200 trays. The energy consumption of this separation process is theoretically estimated about ~12.9 GJ per ton propylene which is much higher than that of ethylene/ethane separation (~7.3 GJ per ton ethylene).[4,5] Therefore, propylene/propane separation is reported as the most capital and energy-intensive distillation process.[6,7] There is a great demand to develop alternative and energy-efficient separation technologies, including adsorptive separation using porous materials.

As emerging porous materials, metal–organic frameworks (MOFs) feature great capability in pore engineering,[8−12] especially precise size-tuning and functionalization of the pore surface, and thus have been explored for gas separation and purification.[13−20] MOFs have been demonstrated as superior adsorbents for many pivotal hydrocarbon separations.[21−26] In terms of olefin/paraffin separation, MOFs with strong binding sites such as open metal sites can selectively adsorb olefin over paraffin through a π-complexation mechanism. But the coadsorption of the paraffin counterpart usually exists and prevents the production of high-purity olefin.[27−30] The second approach is to functionalize MOF pore surfaces for preferential binding of paraffin over olefin, which directly produces pure olefin, as demonstrated in ethane/ethylene separation by a few unique MOFs.[21,31−35] The third approach is to finely tune the pore sizes of MOFs, enabling size exclusion of the large molecule for high sieving separation, as exemplified by few examples.[36−39] Compared with the molecular structure difference between ethylene (C_2H_4) and ethane (C_2H_6), the

Received: September 2, 2020
Published: September 29, 2020

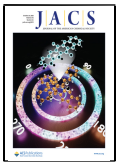

https://dx.doi.org/10.1021/jacs.0c09466
J. Am. Chem. Soc. 2020, 142, 17795−17801

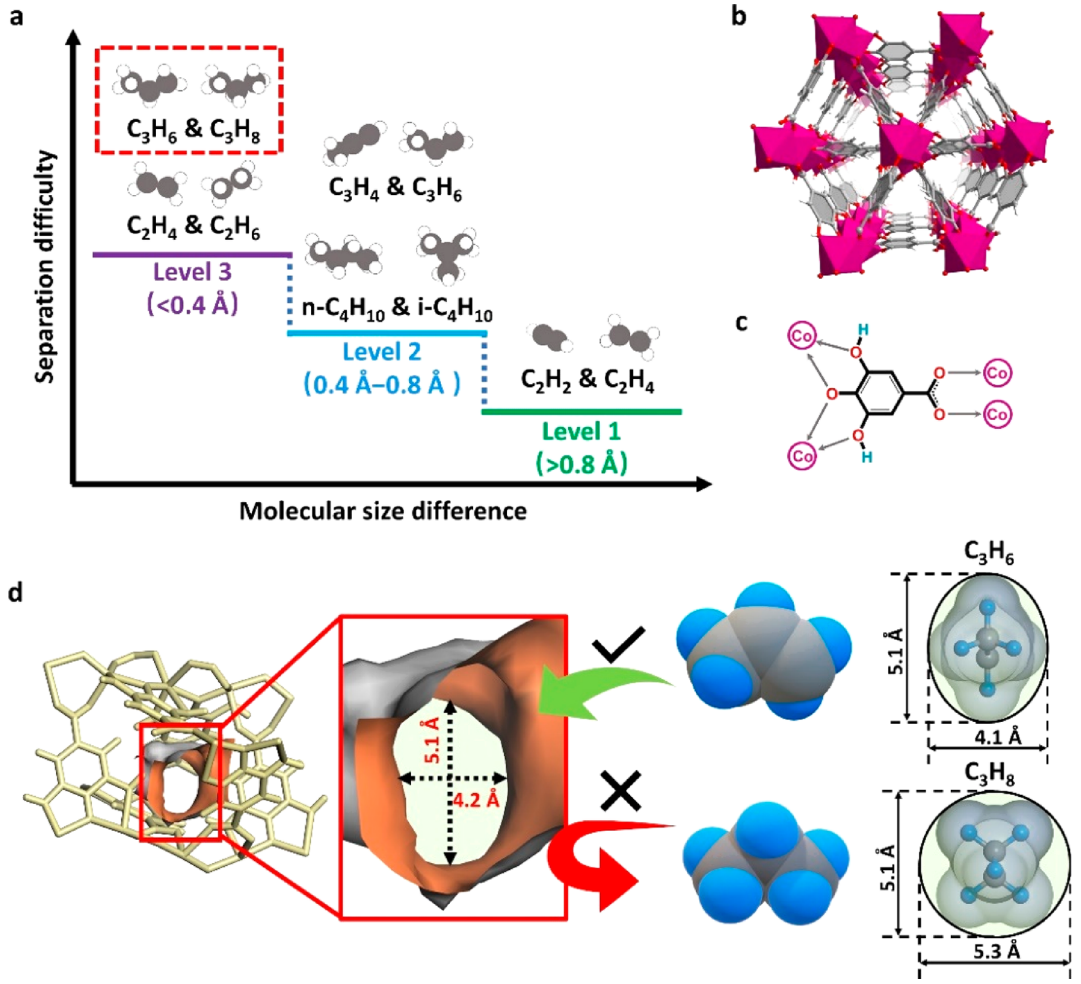

Figure 1. Structure of Co-gallate MOF and rationale for C_3H_6/C_3H_8 separation. (a) The complexity of different hydrocarbon separation systems classified by the molecular size difference. (b) The crystal structure of Co-gallate MOF without guest; purple, red, gray, and white nodes represent Co, O, C, and H atoms, respectively. (c) The coordination mode of the gallate linker. (d) Schematic diagram of the size sieving separation for C_3H_6 and C_3H_8 molecules. Co-gallate MOF shows elliptical pore window with dimensions of 5.1 and 4.2 Å, respectively, which are slightly larger than those of C_3H_6 molecule (5.1 and 4.1 Å, respectively) and smaller than those of C_3H_8 molecule (5.3 and 5.1 Å, respectively).

difference between propylene (C_3H_6) and propane (C_3H_8) molecules is smaller because both molecules have the same alkyl part (i.e., CH_3 group). This smaller difference of molecular structure and size makes either propane-selective separation or propylene sieving separation a more challenging task.[28,29,40,41] In terms of high sieving separation, compared with other separations of alkyne/alkene and branched/linear alkanes, the subtle molecular size difference of olefin and paraffin (below 0.04 nm, i.e. <0.4 Å) makes their separation difficulty at a high level, particularly for C_3H_6/C_3H_8 separation (Figure 1a).

Constructed from a common substance in pharmaceutical industry, gallic acid, a readily available and ultramicroporous MOF Co-gallate was previously reported as high sieving adsorbent for C_2H_4/C_2H_6 separation, that were basically discovered unexpectedly. Here we have carefully analyzed the pore space of this MOF with a discovery of its pore size distribution at 5.2 Å that is between the molecular sizes of propylene and propane, which motivated us to examine its potential for size exclusion of propane from propylene under ambient conditions. The optimal channel size and pore confinement for propylene molecules indeed endows Co-gallate with high sieving separation for propylene from propane with exceptional selectivity. Furthermore, Co-gallate exhibits both high propylene capacity (66.6 cm^3 cm^{-3}, STP) and dynamic separation productivity (36.4 cm^3 cm^{-3}, STP) according to breakthrough experiments under ambient conditions. The Co-gallate MOF exhibits a clear separation mechanism as validated by pore size analyses and crystallographic and modeling studies. Moreover, the facile synthesis and high water stability of this low-cost MOF also highlight its promise for industrial C_3H_6/C_3H_8 separation in the future.

RESULTS AND DISCUSSION

Co-gallate·$2H_2O$ ($[Co(C_7O_5H_4)]\cdot 2H_2O$) was synthesized under hydrothermal reaction of gallic acid and cobalt chloride in aqueous solution. Because gallic acid has good water solubility, water is used here as reaction medium without the use of any harmful organic solvents. Crystallographic studies based on neutron powder diffraction reveals that the activated Co-gallate crystallizes in the $P3_1$ space group, in which each Co^{2+} ion is octahedrally coordinated by two oxygen atoms from two different carboxylate groups, four oxygen atoms from hydroxyl groups, and two deprotonated μ_2-O atoms in two gallate ligands (Figure 1b,c). The CoO_6 octahedra are bridged by the linkers to form rod-like infinite cobalt-oxo chains, which

https://dx.doi.org/10.1021/jacs.0c09466
J. Am. Chem. Soc. 2020, 142, 17795−17801

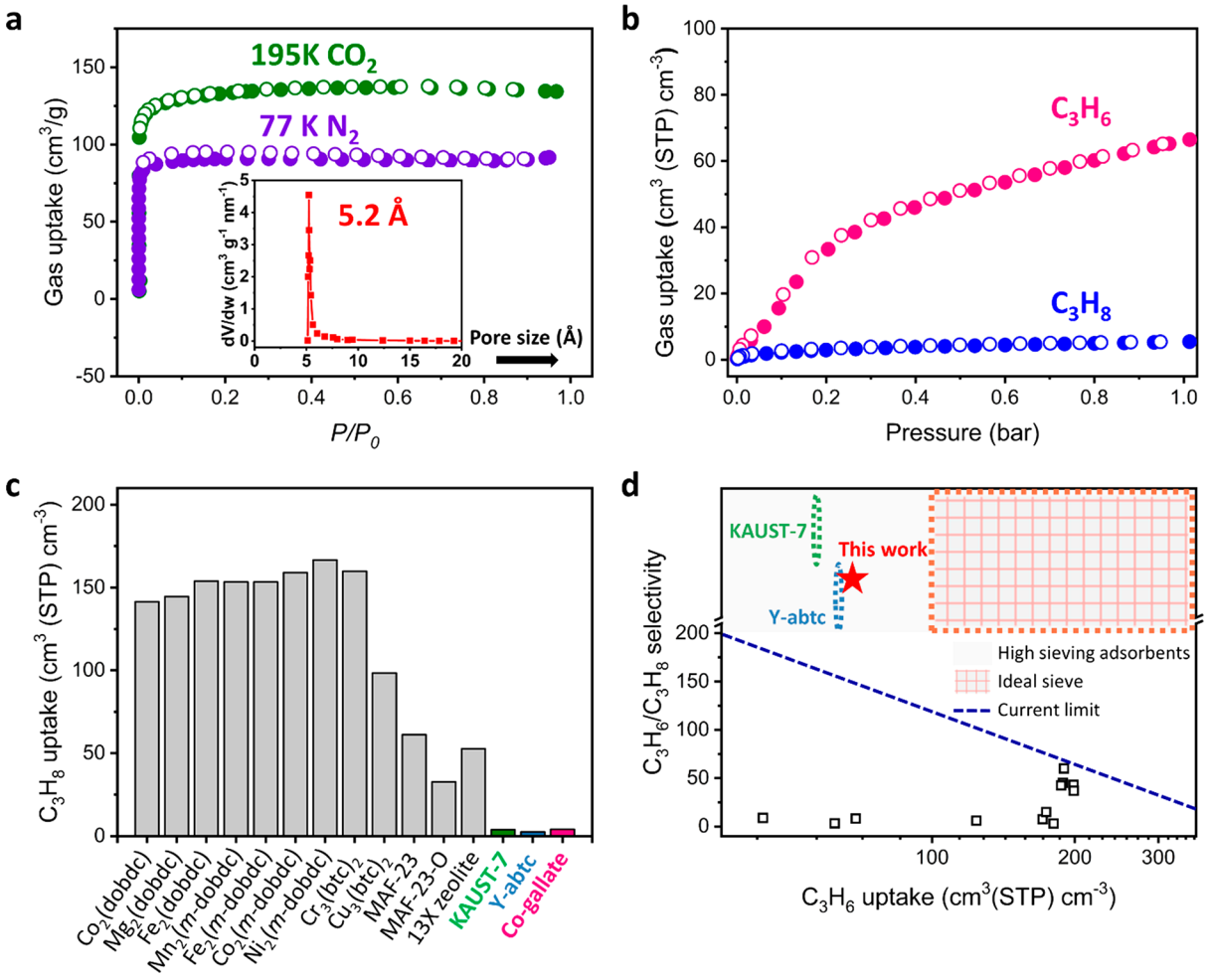

Figure 2. Gas sorption properties of Co-gallate. (a) Single-component sorption isotherms of carbon dioxide at 195 K, nitrogen at 77 K. The inset shows the pore size distribution of Co-gallate MOF (about 5.2 Å) calculated from 77 K N_2 adsorption isotherm based on the Horvath−Kawazoe model. (b) Gas sorption isotherms of propylene and propane at 298 K for Co-gallate. (c) Comparison of propane uptake with reported porous materials.[28,30,37,38,42] (d) Qualitative comparison of adsorption IAST selectivity with uptake of different porous materials for an equimolar propylene/propane mixture.[28,30,37,38,42] IAST selectivity of the MOF sieves is largely uncertain associated with the low uptake of propane. Ideal molecular sieves here are defined as those which can completely block C_3H_8 molecules and take up large amount of C_3H_6 molecules from gas mixtures.

are further interconnected into three-dimensional structure. Co-gallate features a three-dimensional branched channel system interconnected by the narrow window between neighboring ligands along the *c* axis. Notably, the narrow elliptical window shows an aperture size of 16.8 $Å^2$, which is slightly larger than the minimum cross-sectional area of propylene (16.4 $Å^2$) and smaller than that of propane (21.2 $Å^2$) (Figure 1d and Figure S1), indicating a potential shape-sieving effect for propylene from propane in Co-gallate MOF.

Prior to C_3H_6 and C_3H_8 adsorption measurements, the permanent porosity of Co-gallate was examined by CO_2 adsorption at 195 K and N_2 adsorption at 77 K. The CO_2 and N_2 adsorption isotherms of Co-gallate show reversible type-I adsorption profiles. The total CO_2 and N_2 uptake capacities of Co-gallate are 141.1 and 89.6 $cm^3\ g^{-1}$, respectively (Figure 2a). The Brunauer−Emmett−Teller (BET) surface area and pore volume are determined as 486.8 $m^2\ g^{-1}$ and 0.21 $cm^3\ g^{-1}$, respectively, based on the CO_2 adsorption isotherm (Figure S2). Pore size distribution analysis from N_2 adsorption isotherm at 77 K confirms the pore size of Co-gallate MOF is about 5.2 Å, and it is slightly smaller than the molecular size of propane in the elliptic cylinder model, matching well with the size difference between C_3H_6 and C_3H_8.

Motivated by the optimal pore size of Co-gallate MOF, single-component adsorption isotherms at 298 K were collected to evaluate its C_3H_6/C_3H_8 separation performance. A notable amount of propylene was adsorbed by Co-gallate with an uptake capacity of 66.6 $cm^3\ cm^{-3}$ (STP) at 1 bar, which is higher than that of the benchmark niobium-based KAUST-7[37] (56.8 $cm^3\ cm^{-3}$, STP) and yttrium-based Y-abtc[38] (63.5 $cm^3\ cm^{-3}$, STP), owing to the slightly larger pore volume of Co-gallate (Figure 2b). The C_3H_6 adsorption capacity of Ni-gallate and Mg-gallate MOF at 298 K and 1 bar are 47.7 and 54.1 $cm^3\ cm^{-3}$ (STP), respectively (Figure S3). The packing density of C_3H_6 in Co-gallate is calculated to be 0.36 g cm^{-3} (~71% of liquid propylene density). In contrast, Co-gallate only adsorbed a negligible amount of C_3H_8 (5.2 cm^3/cm^3, STP) at 298 K and 1 bar. This low C_3H_8 uptake is very rare among MOFs for C_3H_6/C_3H_8 separation. The C_3H_8 uptake of Co-gallate (5.2 $cm^3\ cm^{-3}$, STP) is about 2 orders of magnitude lower than those of M_2(dobdc) and M_2(*m*-dobdc) (120−163

https://dx.doi.org/10.1021/jacs.0c09466
J. Am. Chem. Soc. 2020, 142, 17795−17801

cm^3 cm^{-3}, STP, Figure 2c and Table S3).[28,30,40,41] The Co-gallate MOF with high sieving effect is very promising for the recovery of high-purity C_3H_6 through a pressure swing adsorption (PSA) process due to the negligible coadsorption of C_3H_8. Notably, there is also no significant C_3H_8 uptake by Co-gallate at different temperatures (273−313 K), whereas the C_3H_6 uptake capacity can further increase to 97.5 cm^3 cm^{-3} (STP) at 273 K (Figures S4 and S5). Based on adsorption isotherms at 273 and 298 K, the isosteric heat of adsorption (Q_{st}) was calculated to be 41 kJ mol^{-1} using the virial method (Figures S6 and S7). The apparent adsorption enthalpy is quite low compared with those of other MOFs (Table S3), which is desirable for facile regeneration under mild conditions.

We employed the ideal adsorbed solution theory (IAST) to evaluate the separation selectivity of a C_3H_6/C_3H_8 mixture. The IAST selectivity was calculated to be 330 at 1 bar and 298 K (Figure 2d and Figure S8), which is much higher than those of many top-performing MOFs, such as Co_2(dobdc) (46), Mn_2(dobdc) (25), Fe_2(*m*-dobdc) (60), Mn_2(*m*-dobdc) (43) (Table S3),[30,40,41] and comparable with those of the benchmark KAUST-7[37] and Y-abtc,[38] implying its potential for highly efficient separation of C_3H_6 from C_3H_8. It should be noted that the IAST selectivity for molecular sieves is often subject to uncertainties due to the large error from the ultralow C_3H_8 uptake.

To structurally understand the separation performance of Co-gallate, high-resolution neutron powder diffraction (NPD) of C_3D_6-loaded Co-gallate MOF was measured to determine the supramolecular interactions between the framework and C_3D_6 molecule (Figure S9). Three types of crystallographically independent C_3D_6 molecules are identified at the intersection of the cross-linking channel system, as shown in Figure 3a. The occupancy of C_3D_6 were refined to be 0.48(2), 0.34(2), and 0.32(2) at sites I, II, and III, respectively, which corresponds to 62.2 cm^3 cm^{-3} (STP), in great agreement with the amount in gas adsorption experiment (66.6 cm^3 cm^{-3}, STP) at 1 bar. The C_3D_6 molecules are confined inside the pore through multiple weak interactions among three sites in slightly different binding geometry (Figure 3b, Figures S10 and S11). Specifically, on site III, C−D···O hydrogen bonding (1.92(4)−3.18(4) Å), O−H···π interaction (2.28(2)- 2.87(1) Å), and weak van der Waals interactions C−D···π (2.61(4)−3.15(5) Å) are observed between C_3D_6 molecule and the hydroxyl group or the aromatic ring on the ligand (Figure 3c−e and Table S5), enabling the C_3D_6 molecules to accommodate well into the pore structure. In addition, the structural comparison of bare Co-gallate and C_3D_6-loaded Co-gallate reveals a negligible framework deformation indicating certain rigidity of Co-gallate framework upon guest molecules inclusion (Figure S12). Therefore, the pore structure enables sufficient diffusion and confinement of C_3H_6 into Co-gallate while showing size exclusion for the slightly larger C_3H_8 molecule.

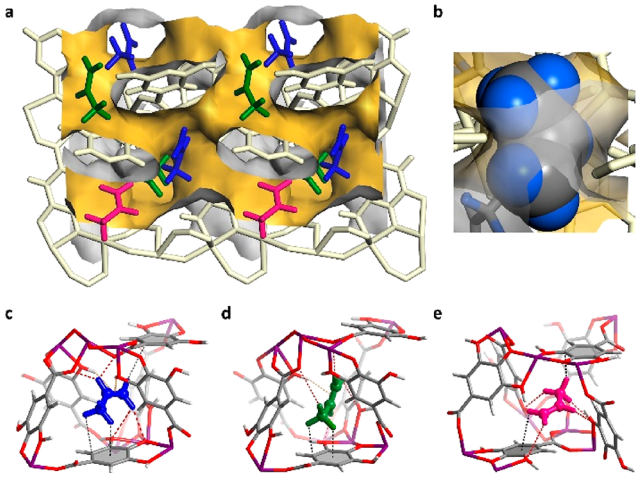

Figure 3. Neutron diffraction crystal structure of Co-gallate·0.38C_3D_6 and preferential binding sites for C_3D_6. (a) The packing diagram of the C_3D_6 absorbed structure. The preferential binding sites for C_3D_6 (site I, site II, and site III) are represented in blue, green, and pink, respectively. The framework and the pore surface are shown in pale gold and yellow. (b) View of the optimal aperture of Co-gallate MOF for exact confinement of propylene molecules. The light blue and gray spheres represent H and C atoms of propylene molecules. (c−e) Three different preferential adsorption sites, site I (c), site II (d), and site III (e), and their close contacts with the framework, with C−D···O, C−D···π, and O−H···π interactions highlighted as red, black, and orange dashed lines, respectively.

Motivated by the C_3H_8-exclusion of Co-gallate shown by single component adsorption, we further evaluated its C_3H_6/C_3H_8 separation performance by transient breakthrough simulation, in comparison with several benchmark materials (Figure S13). The simulated breakthrough curve shows that the retention time of C_3H_8 in Co-gallate is negligible as the result of molecular exclusion. In contrast, the retention time of C_3H_8 for M_2(*m*-dobdc) and M_2(dobdc) series are much longer due to their significant coadsorption of C_3H_8 (Figures S14 and S15). Co-gallate also exhibits much higher dynamic selectivity and purity of C_3H_6 in adsorbed phase based on the transient breakthrough curve (Figure S16 and Table S4). Next, we carried out binary gas (50/50 C_3H_6/C_3H_8) column breakthrough measurements (Figure S17). C_3H_8 eluted at the very beginning of the process, indicating no noticeable adsorption of C_3H_8 in the column (Figure 4a) whereas C_3H_6 underwent a long retention time of ∼28 min. Correspondingly, the dynamic propylene productivity was calculated to be 36.4 cm^3 cm^{-3} (STP) (Figure S18), which is higher than that of niobium-based KAUST-7[37] (26.3 cm^3 cm^{-3}, STP) and comparable to that of yttrium-based Y-abtc[38] (41.1 cm^3 cm^{-3}, STP). Compared with the equilibrium capacity for C_3H_6 at 0.5 bar, the lower dynamic C_3H_6 adsorption capacity of Co-gallate may be attributed to the relatively slow diffusion of C_3H_6 into the pore channels during the separation process (Figure S19). The adsorbed propylene can be simply desorbed in 14 min by purging pure He gas at room temperature. A small amount of C_3H_8 was detected in the desorbed gas, and the purity of C_3H_6 was calculated to be 97.7% through a single PSA process (Figure 4b and Figure S20). The mild desorption condition can further reduce energy cost as compared to zeolite 4A which requires high desorption temperature.[43] To examine the reusability of Co-gallate in multiple cycling separation, five regeneration-breakthrough cycles were performed, and its dynamic productivity was fully retained (Figure 4c, Figures S21 and S22).

Under practical conditions, the C_3H_6/C_3H_8 mixtures may contain small amount of other gas impurities including methane and ethane.[44,45] The effect of these impurities on the separation performance was investigated by a breakthrough experiment of quaternary gas mixture $CH_4/C_2H_6/C_3H_6/C_3H_8$ (5/5/45/45, v/v/v/v). As expected, Co-gallate can adsorb C_3H_6 from the mixture exclusively and CH_4, C_2H_6, and C_3H_8 eluted in the first 2 min. The breakthrough result indicates that

https://dx.doi.org/10.1021/jacs.0c09466
J. Am. Chem. Soc. 2020, 142, 17795−17801

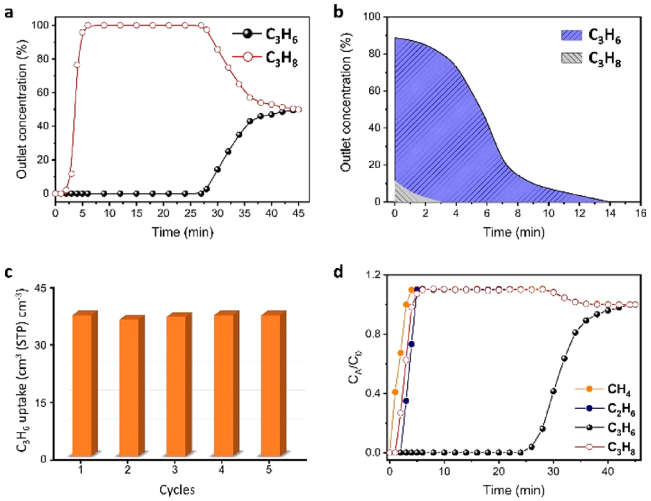

Figure 4. Column breakthrough results of Co-gallate MOF. (a) Breakthrough curves for Co-gallate MOF for an equimolar binary mixture of C_3H_6/C_3H_8 at 298 K and 1 bar. The breakthrough experiments were carried out in a packed column with 1.26 g sample at a flow rate of 1.7 mL min^{-1}. The points are experimental data, and the lines are drawn to guide the eye. (b) Concentration curve of the desorbed C_3H_6 from Co-gallate during the regeneration process. (c) Dynamic adsorption capacity of Co-gallate for C_3H_6 with five breakthrough experimental cycles. (d) Multicomponent breakthrough curves for a quaternary mixture of $CH_4/C_2H_6/C_3H_6/C_3H_8$ (5/5/45/45) at 298 K and 1 bar. The points are experimental data, and the lines are drawn to guide the eye.

Co-gallate is a very promising absorbent for propylene recovery from multicomponent gas streams (Figure 4d and Figure S23). Considering that the material stability is very important in practical application, powder X-ray diffraction (PXRD) and gas adsorption measurements of Co-gallate were carried out after immersion in water for 7 days to examine its water stability. The PXRD result shows that the crystallinity of Co-gallate was retained upon water immersion (Figure S24). Moreover, the C_3H_6 and C_3H_8 adsorption measurements reveal that the adsorption capacity and selectivity of the water-soaked Co-gallate remain unchanged (Figures S25–29). The above results demonstrate that Co-gallate material is highly stable in water. The as-synthesized Co-gallate MOFs do not show framework decomposition until approximately 280 °C (Figure S30). In addition, Co-gallate can be obtained at low cost from inexpensive and readily available chemicals via a green synthetic method using only water as the solvent. Such low production cost and high sieving separation of propylene from propane endow Co-gallate with excellent potential for industrial applications.

CONCLUSIONS

In summary, by virtue of optimal pore structure and surface functionalities of MOF materials, challenging gas separations of different complexities can be realized. For the important C_3H_6/C_3H_8 separation, the above results illustrate that high sieving separation is a highly efficient approach to minimize the coadsorption of impurity components and boost the product purity. In this context, ultramicroporous MOFs featuring pore confinement and pore size matching represent potential adsorbent candidates, although there are still concerns on their separation capacity limit, material cost, and scalable synthesis. Overall, continuous research efforts on exploring superior adsorbents for advanced adsorptive separation technologies would reap great energy benefits.

ASSOCIATED CONTENT

Supporting Information

The Supporting Information is available free of charge at https://pubs.acs.org/doi/10.1021/jacs.0c09466.

CIF data for Co-gallate (CIF)

CIF data for Co-gallate·C_3D_6 (CIF)

Experimental procedures, additional figures, characterizations, and additional tables (PDF)

AUTHOR INFORMATION

Corresponding Authors

Rui-Biao Lin − *Department of Chemistry, University of Texas at San Antonio, San Antonio, Texas 78249-0698, United States;* orcid.org/0000-0003-3267-220X; Email: ruibiao.lin@utsa.edu

Wei Zhou − *NIST Center for Neutron Research, Gaithersburg, Maryland 20899-6102, United States;* orcid.org/0000-0002-5461-3617; Email: wzhou@nist.gov

Banglin Chen − *Department of Chemistry, University of Texas at San Antonio, San Antonio, Texas 78249-0698, United States;* orcid.org/0000-0001-8707-8115; Email: banglin.chen@utsa.edu

Authors

Bin Liang − *Department of Chemistry, University of Texas at San Antonio, San Antonio, Texas 78249-0698, United States*

Xin Zhang − *Department of Chemistry, University of Texas at San Antonio, San Antonio, Texas 78249-0698, United States;* orcid.org/0000-0001-9318-8839

Yi Xie − *Department of Chemistry, University of Texas at San Antonio, San Antonio, Texas 78249-0698, United States*

Rajamani Krishna − *Van't Hoff Institute for Molecular Sciences, University of Amsterdam, 1098, XH, Amsterdam, The Netherlands;* orcid.org/0000-0002-4784-8530

Hui Cui − *Department of Chemistry, University of Texas at San Antonio, San Antonio, Texas 78249-0698, United States;* orcid.org/0000-0002-9723-4932

Zhiqiang Li − *Department of Chemistry, University of Texas at San Antonio, San Antonio, Texas 78249-0698, United States; School of Chemical Engineering and Technology, Hebei University of Technology, Tianjin 300130, P. R. China;* orcid.org/0000-0001-6901-4281

Yanshu Shi − *Department of Chemistry, University of Texas at San Antonio, San Antonio, Texas 78249-0698, United States*

Hui Wu − *NIST Center for Neutron Research, Gaithersburg, Maryland 20899-6102, United States;* orcid.org/0000-0003-0296-5204

Complete contact information is available at: https://pubs.acs.org/10.1021/jacs.0c09466

Author Contributions

[§]B.L and X.Z contributed equally to this work.

Notes

The authors declare no competing financial interest.

ACKNOWLEDGMENTS

We acknowledge financial support from the Welch Foundation (AX-1730).

REFERENCES

(1) Sholl, D. S.; Lively, R. P. Seven chemical separations to change the world. *Nature* **2016**, *532* (7600), 435−437.

(2) Lin, J. Y. S. Molecular sieves for gas separation. *Science* **2016**, *353* (6295), 121−122.

(3) Christopher, C. C. E.; Dutta, A.; Farooq, S.; Karimi, I. A. Process synthesis and optimization of propylene/propane separation using vapor recompression and self-heat recuperation. *Ind. Eng. Chem. Res.* **2017**, *56* (49), 14557−14564.

(4) Worrell, E.; Phylipsen, D.; Einstein, D.; Martin, N., *Energy use and energy intensity of the u.s. chemical industry*. https://www.energystar.gov, 2000.

(5) Li, K.; Beaver, M., *Advanced nanostructured molecular sieves for energy efficient industrial separations*. https://www.semanticscholar.org, 2012.

(6) Chu, S.; Cui, Y.; Liu, N. The path towards sustainable energy. *Nat. Mater.* **2017**, *16* (1), 16−22.

(7) Järvelin, H.; Fair, J. R. Adsorptive separation of propylene-propane mixtures. *Ind. Eng. Chem. Res.* **1993**, *32* (10), 2201−2207.

(8) Furukawa, H.; Cordova, K. E.; O'Keeffe, M.; Yaghi, O. M. The chemistry and applications of metal-organic frameworks. *Science* **2013**, *341* (6149), 1230444.

(9) Zhao, X.; Wang, Y.; Li, D. S.; Bu, X.; Feng, P. Metal-Organic Frameworks for Separation. *Adv. Mater.* **2018**, *30* (37), 1705189.

(10) Li, H.; Li, L.; Lin, R.-B.; Zhou, W.; Zhang, Z.; Xiang, S.; Chen, B. Porous metal-organic frameworks for gas storage and separation: Status and challenges. *EnergyChem.* **2019**, *1* (1), 100006.

(11) Ye, Y.; Ma, Z.; Lin, R. B.; Krishna, R.; Zhou, W.; Lin, Q.; Zhang, Z.; Xiang, S.; Chen, B. Pore Space Partition within a Metal-Organic Framework for Highly Efficient C_2H_2/CO_2 separation. *J. Am. Chem. Soc.* **2019**, *141* (9), 4130−4136.

(12) Liang, C.-C.; Shi, Z.-L.; He, C.-T.; Tan, J.; Zhou, H.-D.; Zhou, H.-L.; Lee, Y.; Zhang, Y.-B. Engineering of pore geometry for ultrahigh capacity methane storage in mesoporous metal-organic frameworks. *J. Am. Chem. Soc.* **2017**, *139* (38), 13300−13303.

(13) Zhou, D.-D.; Chen, P.; Wang, C.; Wang, S.-S.; Du, Y.; Yan, H.; Ye, Z.-M.; He, C.-T.; Huang, R.-K.; Mo, Z.-W.; Huang, N.-Y.; Zhang, J.-P. Intermediate-sized molecular sieving of styrene from larger and smaller analogues. *Nat. Mater.* **2019**, *18* (9), 994−998.

(14) Hao, H.-G.; Zhao, Y.-F.; Chen, D.-M.; Yu, J.-M.; Tan, K.; Ma, S.; Chabal, Y.; Zhang, Z.-M.; Dou, J.-M.; Xiao, Z.-H.; Day, G.; Zhou, H.-C.; Lu, T.-B. Simultaneous trapping of C_2H_2 and C_2H_6 from a Ternary Mixture of $C_2H_2/C_2H_4/C_2H_6$ in a robust metal-organic framework for the purification of C_2H_4. *Angew. Chem., Int. Ed.* **2018**, *57* (49), 16067−16071.

(15) Gu, C.; Hosono, N.; Zheng, J.-J.; Sato, Y.; Kusaka, S.; Sakaki, S.; Kitagawa, S. Design and control of gas diffusion process in a nanoporous soft crystal. *Science* **2019**, *363* (6425), 387−391.

(16) Li, J.-R.; Sculley, J.; Zhou, H.-C. Metal-organic frameworks for separations. *Chem. Rev.* **2012**, *112* (2), 869−932.

(17) Yoon, J. W.; Chang, H.; Lee, S. J.; Hwang, Y. K.; Hong, D. Y.; Lee, S. K.; Lee, J. S.; Jang, S.; Yoon, T. U.; Kwac, K.; Jung, Y.; Pillai, R. S.; Faucher, F.; Vimont, A.; Daturi, M.; Ferey, G.; Serre, C.; Maurin, G.; Bae, Y. S.; Chang, J. S. Selective nitrogen capture by porous hybrid materials containing accessible transition metal ion sites. *Nat. Mater.* **2017**, *16* (5), 526−531.

(18) Krause, S.; Bon, V.; Senkovska, I.; Stoeck, U.; Wallacher, D.; Tobbens, D. M.; Zander, S.; Pillai, R. S.; Maurin, G.; Coudert, F. X.; Kaskel, S. A pressure-amplifying framework material with negative gas adsorption transitions. *Nature* **2016**, *532* (7599), 348−352.

(19) Foo, M. L.; Matsuda, R.; Hijikata, Y.; Krishna, R.; Sato, H.; Horike, S.; Hori, A.; Duan, J.; Sato, Y.; Kubota, Y.; Takata, M.; Kitagawa, S. An adsorbate discriminatory gate effect in a flexible porous coordination polymer for selective adsorption of CO_2 over C_2H_2. *J. Am. Chem. Soc.* **2016**, *138* (9), 3022−30.

(20) Lin, R.-B.; Xiang, S.; Zhou, W.; Chen, B. Microporous metal-organic framework materials for gas separation. *Chem.* **2020**, *6* (2), 337−363.

(21) Zeng, H.; Xie, X.-J.; Xie, M.; Huang, Y.-L.; Luo, D.; Wang, T.; Zhao, Y.; Lu, W.; Li, D. Cage-interconnected metal-organic framework with tailored apertures for efficient C_2H_6/C_2H_4 separation under humid conditions. *J. Am. Chem. Soc.* **2019**, *141* (51), 20390−20396.

(22) Cui, X.; Chen, K.; Xing, H.; Yang, Q.; Krishna, R.; Bao, Z.; Wu, H.; Zhou, W.; Dong, X.; Han, Y.; Li, B.; Ren, Q.; Zaworotko, M. J.; Chen, B. Pore chemistry and size control in hybrid porous materials for acetylene capture from ethylene. *Science* **2016**, *353* (6295), 141−144.

(23) Chen, K.-J.; Madden, D. G.; Mukherjee, S.; Pham, T.; Forrest, K. A.; Kumar, A.; Space, B.; Kong, J.; Zhang, Q.-Y.; Zaworotko, M. J. Synergistic sorbent separation for one-step ethylene purification from a four-component mixture. *Science* **2019**, *366* (6462), 241−246.

(24) Peng, Y.-L.; He, C.; Pham, T.; Wang, T.; Li, P.; Krishna, R.; Forrest, K. A.; Hogan, A.; Suepaul, S.; Space, B.; Fang, M.; Chen, Y.; Zaworotko, M. J.; Li, J.; Li, L.; Zhang, Z.; Cheng, P.; Chen, B. Robust microporous metal-organic frameworks for highly efficient and simultaneous removal of propyne and propadiene from propylene. *Angew. Chem., Int. Ed.* **2019**, *58* (30), 10209−10214.

(25) Yang, L.; Cui, X.; Yang, Q.; Qian, S.; Wu, H.; Bao, Z.; Zhang, Z.; Ren, Q.; Zhou, W.; Chen, B.; Xing, H. A single-molecule propyne trap: highly efficient removal of propyne from propylene with anion-pillared ultramicroporous materials. *Adv. Mater.* **2018**, *30* (10), 1705374.

(26) Li, L.; Lin, R.-B.; Krishna, R.; Wang, X.; Li, B.; Wu, H.; Li, J.; Zhou, W.; Chen, B. Flexible-robust metal-organic framework for efficient removal of propyne from propylene. *J. Am. Chem. Soc.* **2017**, *139* (23), 7733−7736.

(27) Li, B.; Zhang, Y.; Krishna, R.; Yao, K.; Han, Y.; Wu, Z.; Ma, D.; Shi, Z.; Pham, T.; Space, B.; Liu, J.; Thallapally, P. K.; Liu, J.; Chrzanowski, M.; Ma, S. Introduction of π-complexation into porous aromatic framework for highly selective adsorption of ethylene over ethane. *J. Am. Chem. Soc.* **2014**, *136* (24), 8654−8660.

(28) Bloch, E. D.; Queen, W. L.; Krishna, R.; Zadrozny, J. M.; Brown, C. M.; Long, J. R. Hydrocarbon separations in a metal-organic framework with open iron(II) coordination sites. *Science* **2012**, *335* (6076), 1606−1610.

(29) Yang, S.; Ramirez-Cuesta, A. J.; Newby, R.; Garcia-Sakai, V.; Manuel, P.; Callear, S. K.; Campbell, S. I.; Tang, C. C.; Schroder, M. Supramolecular binding and separation of hydrocarbons within a functionalized porous metal-organic framework. *Nat. Chem.* **2015**, *7* (2), 121−129.

(30) Bae, Y. S.; Lee, C. Y.; Kim, K. C.; Farha, O. K.; Nickias, P.; Hupp, J. T.; Nguyen, S. T.; Snurr, R. Q. High propene/propane selectivity in isostructural metal-organic frameworks with high densities of open metal sites. *Angew. Chem., Int. Ed.* **2012**, *51* (8), 1857−1860.

(31) Li, L.; Lin, R.-B.; Krishna, R.; Li, H.; Xiang, S.; Wu, H.; Li, J.; Zhou, W.; Chen, B. Ethane/ethylene separation in a metal-organic framework with iron-peroxo sites. *Science* **2018**, *362* (6413), 443−446.

(32) Yang, H.; Wang, Y.; Krishna, R.; Jia, X.; Wang, Y.; Hong, A. N.; Dang, C.; Castillo, H. E.; Bu, X.; Feng, P. Pore-space-partition-enabled exceptional ethane uptake and ethane-selective ethane-ethylene separation. *J. Am. Chem. Soc.* **2020**, *142* (5), 2222−2227.

(33) Qazvini, O. T.; Babarao, R.; Shi, Z. L.; Zhang, Y. B.; Telfer, S. G. A robust ethane-trapping metal-organic framework with a high capacity for ethylene purification. *J. Am. Chem. Soc.* **2019**, *141* (12), 5014−5020.

(34) Liao, P.-Q.; Zhang, W.-X.; Zhang, J.-P.; Chen, X.-M. Efficient purification of ethene by an ethane-trapping metal-organic framework. *Nat. Commun.* **2015**, *6*, 8697.

(35) Lin, R.-B.; Wu, H.; Li, L.; Tang, X.-L.; Li, Z.; Gao, J.; Cui, H.; Zhou, W.; Chen, B. Boosting ethane/ethylene separation within isoreticular ultramicroporous metal-organic frameworks. *J. Am. Chem. Soc.* **2018**, *140* (40), 12940−12946.

(36) Bao, Z.; Wang, J.; Zhang, Z.; Xing, H.; Yang, Q.; Yang, Y.; Wu, H.; Krishna, R.; Zhou, W.; Chen, B.; Ren, Q. Molecular sieving of

https://dx.doi.org/10.1021/jacs.0c09466
J. Am. Chem. Soc. 2020, 142, 17795−17801

ethane from ethylene through the molecular cross-section size differentiation in gallate-based metal-organic frameworks. *Angew. Chem., Int. Ed.* **2018**, *57* (49), 16020−16025.
(37) Cadiau, A.; Adil, K.; Bhatt, P. M.; Belmabkhout, Y.; Eddaoudi, M. A metal-organic framework-based splitter for separating propylene from propane. *Science* **2016**, *353* (6295), 137−140.
(38) Wang, H.; Dong, X.; Colombo, V.; Wang, Q.; Liu, Y.; Liu, W.; Wang, X.-L.; Huang, X.-Y.; Proserpio, D. M.; Sironi, A.; Han, Y.; Li, J. Tailor-made microporous metal-organic frameworks for the full separation of propane from propylene through selective size exclusion. *Adv. Mater.* **2018**, *30* (49), e1805088.
(39) Lin, R.-B.; Li, L.; Zhou, H. L.; Wu, H.; He, C.; Li, S.; Krishna, R.; Li, J.; Zhou, W.; Chen, B. Molecular sieving of ethylene from ethane using a rigid metal-organic framework. *Nat. Mater.* **2018**, *17* (12), 1128−1133.
(40) Geier, S. J.; Mason, J. A.; Bloch, E. D.; Queen, W. L.; Hudson, M. R.; Brown, C. M.; Long, J. R. Selective adsorption of ethylene over ethane and propylene over propane in the metal−organic frameworks M2(dobdc) (M = Mg, Mn, Fe, Co, Ni, Zn). *Chem. Sci.* **2013**, *4* (5), 2054−2061.
(41) Bachman, J. E.; Kapelewski, M. T.; Reed, D. A.; Gonzalez, M. I.; Long, J. R. M_2(m-dobdc) (M = Mn, Fe, Co, Ni) metal-organic frameworks as highly selective, high-capacity adsorbents for olefin/paraffin separations. *J. Am. Chem. Soc.* **2017**, *139* (43), 15363−15370.
(42) Wang, Y.; Huang, N.-Y.; Zhang, X.-W.; He, H.; Huang, R.-K.; Ye, Z.-M.; Li, Y.; Zhou, D.-D.; Liao, P.-Q.; Chen, X.-M.; Zhang, J.-P. Selective aerobic oxidation of a metal-organic framework boosts thermodynamic and kinetic propylene/propane selectivity. *Angew. Chem., Int. Ed.* **2019**, *58* (23), 7692−7696.
(43) Rege, S. U.; Padin, J.; Yang, R. T. Olefin/paraffin separations by adsorption: π-complexation vs. kinetic separation. *AIChE J.* **1998**, *44* (4), 799−809.
(44) Sadrameli, S. M. Thermal/catalytic cracking of hydrocarbons for the production of olefins: A state-of-the-art review I: Thermal cracking review. *Fuel* **2015**, *140*, 102−115.
(45) Bai, S.; Sridhar, S.; Khan, A. A. Recovery of propylene from refinery off-gas using metal incorporated ethylcellulose membranes. *J. Membr. Sci.* **2000**, *174* (1), 67−79.

https://dx.doi.org/10.1021/jacs.0c09466
J. Am. Chem. Soc. 2020, 142, 17795−17801

Supporting Information

An Ultramicroporous Metal-Organic Framework for High Sieving Separation of Propylene from Propane

Bin Liang,[†,§] Xin Zhang,[†,§] Yi Xie,[†] Rui-Biao Lin,[*,†] Rajamani Krishna,[∥] Hui Cui,[†] Zhiqiang Li,[†,‡] Yanshu Shi,[†] Hui Wu,[∇] Wei Zhou[*,∇] and Banglin Chen[*,†]

† Department of Chemistry, University of Texas at San Antonio, One UTSA Circle, San Antonio, Texas 78249-0698, United States.

∥ Van't Hoff Institute for Molecular Sciences, University of Amsterdam, Science Park 904, 1098 XH Amsterdam, The Netherlands.

‡ School of Chemical Engineering and Technology, Hebei University of Technology, Tianjin 300130, P. R. China.

∇NIST Center for Neutron Research, Gaithersburg, MD 20899-6102, United States.

*Correspondence to: ruibiao.lin@utsa.edu, wzhou@nist.gov, banglin.chen@utsa.edu

Experimental Procedures

Synthesis of Co-gallate: The synthesis of the Co-gallate sample was performed following the previous report with minor modifications.[1] Gallic acid monohydrate (2 mmol) and $CoCl_2 \cdot 6H_2O$ (1 mmol) and were mixed in 10 mL KOH aqueous solution (0.05 M). The mixture was sealed in a Teflon-lined stainless-steel autoclave first. Then, the autoclave was heated at 120 ^oC for 24 h under autogenous pressure. The autoclave was cooled down at room temperature and the obtained Co-gallate sample was washed with deionized water followed by absolute ethanol.

X-ray diffraction analysis of powder samples: Powder X-ray diffraction patterns were collected by a Rigaku Ultima IV diffractometer (Cu Kα λ= 1.540598 Å) with an operating power of 40 kV, 44 mA and a scan rate of 8.0 °/min. The data were collected in the range of 2θ= 8-50°.

Thermal gravimetric analysis: Thermal gravimetric analysis (TGA) was conducted in a TA-Q500 TGA instrument (TA Instruments Corp., USA) from 30 to 800 ^oC in N_2 at a constant rate of 10 ^oC/min.

Single-component gas sorption measurement: The gas sorption isotherms were collected on an automatic volumetric adsorption apparatus (Micromeritics ASAP 2020 surface area analyzer). The as-synthesized sample was activated at 80 ^oC for 24 h, then 100 ^oC for 24 h, and 120 ^oC for 24 h under ultrahigh vacuum before single-component gas adsorption to remove the guest molecules.

Fitting of pure-component isotherms: The data of pure-component isotherm for C_3H_6 and C_3H_8 in Co-gallate were fitted with the single-site Langmuir-Freundlich model.

$$\mathrm{N} = N_{max}\frac{b_1 \cdot p^{c_1}}{1 + b_1 \cdot p^{c_1}}$$

where p (unit: kPa) is the pressure of the bulk gas at equilibrium with the adsorbed phase, N (unit: mmol g^{-1}) is the adsorbed amount per mass of adsorbent, N_{max} (unit: mmol/g) is the saturation capacities, b (unit: 1/kPa) is the affinity coefficient and n represents the deviation from an ideal homogeneous surface.

Isosteric heat of adsorption: The binding energy of C_3H_6 is reflected in the isosteric heat of adsorption, Q_{st}. The Clausius-Clapeyron equation was employed to calculate the enthalpies of C_3H_6 adsorption:

$$\frac{\partial(Ln\,P)}{\partial(1/T)} = -\frac{Q_{st}}{R}$$

where P is the pressure, T is the temperature and R is the universal gas constant. Adsorption heats (Q_{st}) of Co-gallate for propylene reported here are estimated using pure-component isotherms collected at 273 and 298 K.

IAST calculations of adsorption selectivity: The adsorption selectivity for C_3H_6/ C_3H_8

separation is defined by

$$S_{ads} = \frac{q_1/q_2}{p_1/p_2}$$

q_1 and q_2 are the molar loadings in the adsorbed phase in equilibrium with the bulk gas phase with partial pressures p_1 and p_2.

Breakthrough separation experiments: The breakthrough experiments were conducted in a dynamic gas breakthrough set-up. A stainless-steel column with inner dimensions of 4 mm and a length of 81 mm was used for sample packing. The activated sample (1.26 g) was then packed into the column. The flow and pressure of binary gas (C_3H_6/C_3H_8 at 50/50, v/v) were controlled by using a pressure control valve and a mass flow controller. The outlet effluent from the column was continuously monitored by gas chromatography (GC-2014, Shimadzu) with a thermal conductivity detector. The column packed with activated sample was first purged with helium gas flow for 1 h at room temperature. The gas mixtures flow rate is 1.7 ml/min at 1 bar during the breakthrough process. After the breakthrough experiment, the sample was regenerated with helium gas flow (60 ml/min) for about 14 min at 298 K.

Transient breakthrough of C_3H_6/C_3H_8 mixtures in fixed-bed absorbers: For comparison with breakthrough experiments with Co-gallate, transient breakthrough simulations were undertaken using the same methodology as discussed in earlier publications.[2] The dimensions parameter, including breakthrough tube, sample mass and flow rates, were selected to match the experimental conditions precisely. The breakthrough times of C_3H_8 and C_3H_6 can be captured reasonably accurately. The simulated breakthroughs are sharper than those observed experimentally due to the intracrystalline diffusional influences are ignored in the simulations. The distended characteristics of the experimental breakthroughs with Co-gallate are because of finite diffusional resistances. We investigated the separation performance of Co-gallate for separation of a C_3H_6/C_3H_8 feed mixture (50/50, v/v). The total bulk gas phase is at 298 K and 100 kPa. The dynamic selectivity and purity are calculated based on the integration proportion of transient breakthrough simulations curves.

Additional Figure

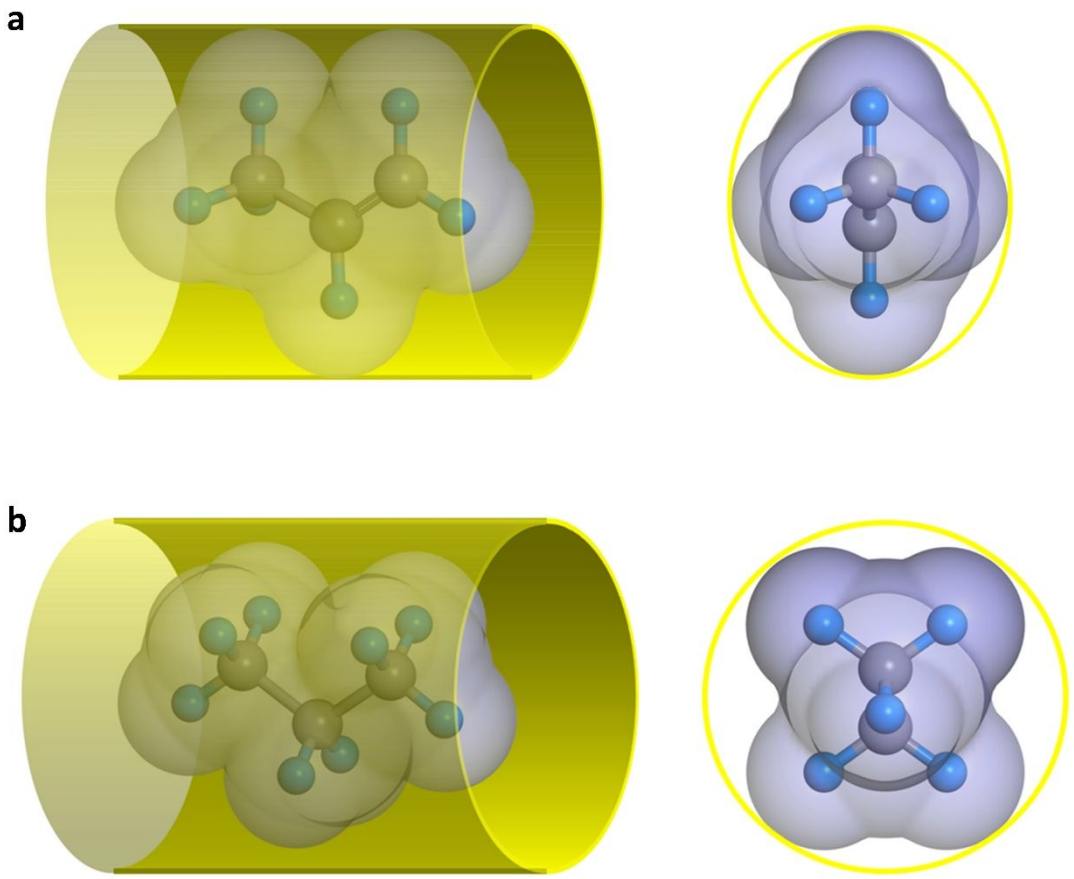

Figure S1. For the elliptical channels, the minimum cross-sectional area of propylene (a) and propane (b) are 16.4 $Å^2$ and 21.2 $Å^2$, respectively. The minimum cross-sectional areas can be calculated from the minimum molecular dimensions.[3]

Characterizations

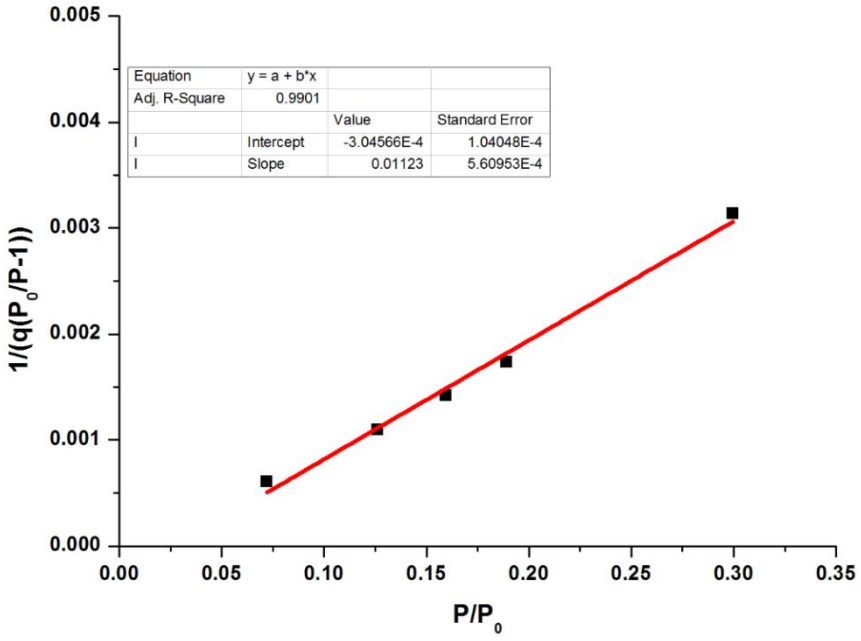

Figure S2. Calculation of BET surface area for Co-gallate based on CO_2 adsorption isotherm at 195 K.

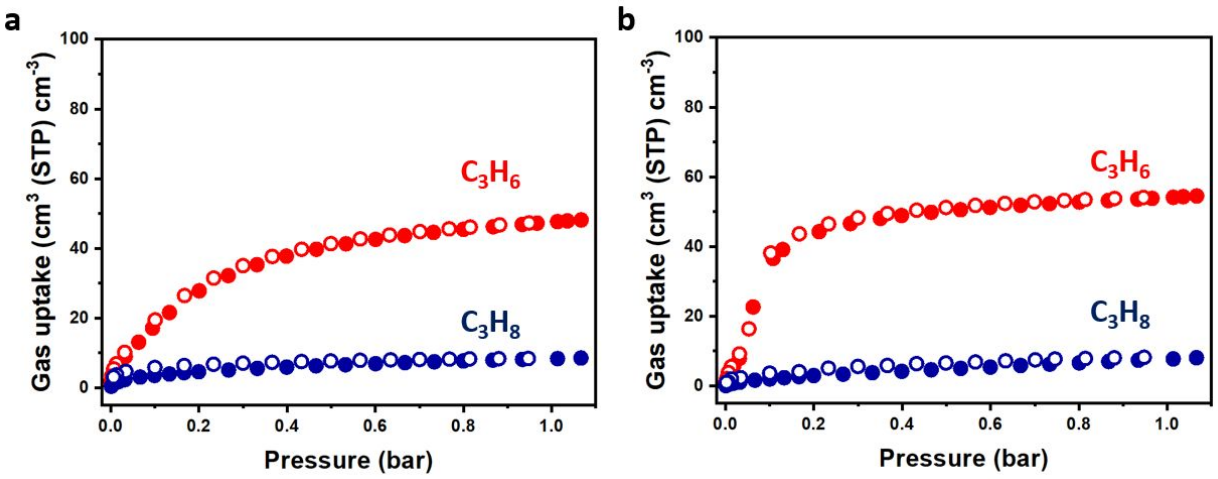

Figure S3. Single-component adsorption isotherms for C_3H_6 and C_3H_8 for (a) Ni-gallate, and (b) Mg-gallate at 298 K.

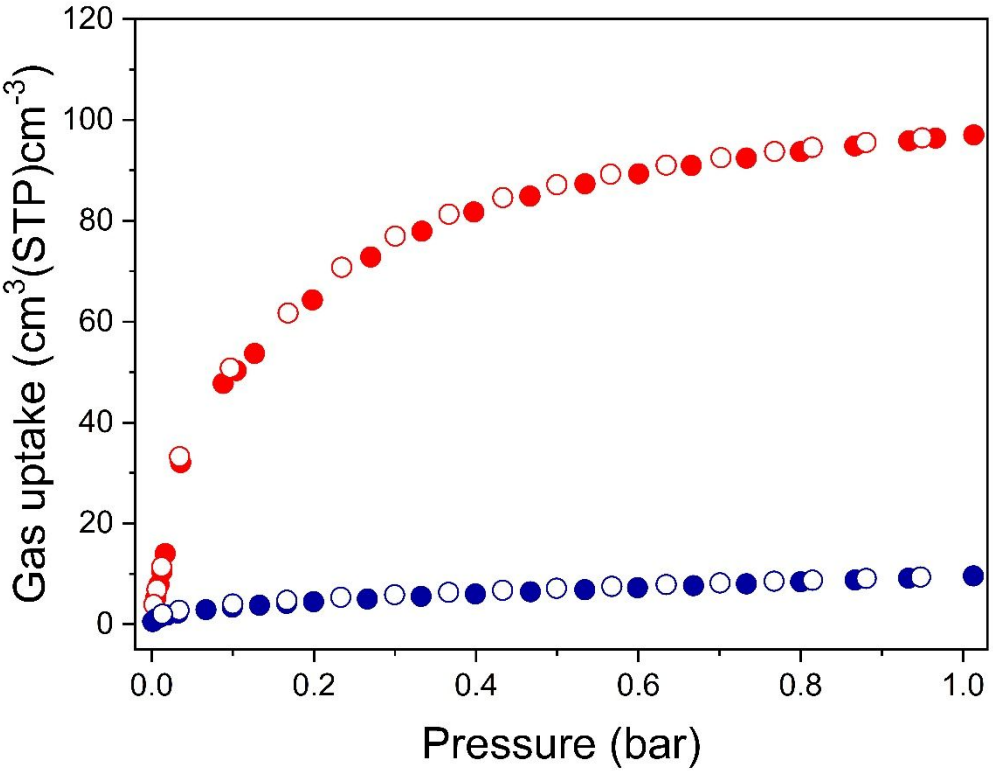

Figure S4. Sorption isotherms of Co-gallate for C_3H_6 (Red) and C_3H_8 (blue) at 273K.

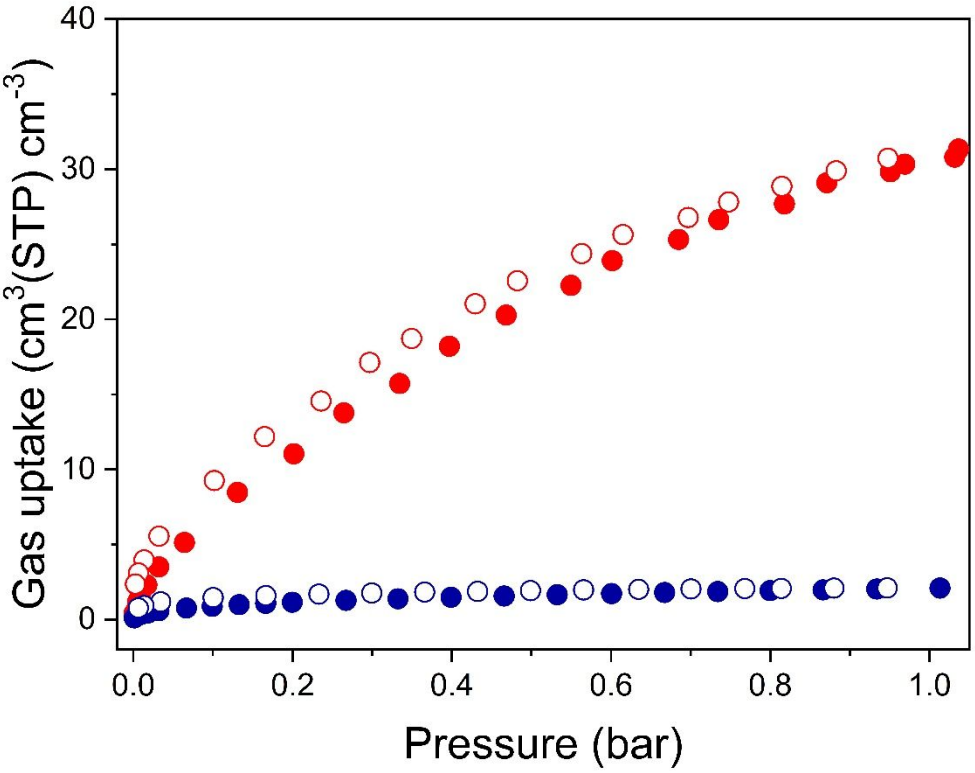

Figure S5. Sorption isotherms of Co-gallate for C_3H_6 (red) and C_3H_8 (blue) at 313K.

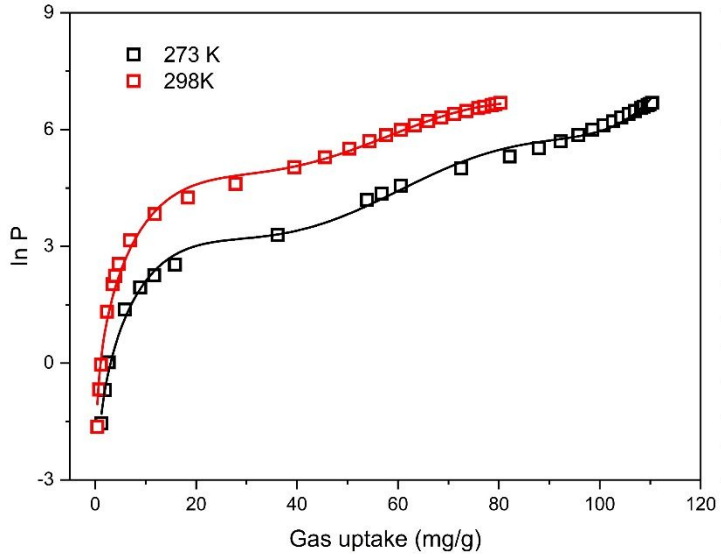

Model	Qst
Equation	y = ln(x)+1/T*(a0+a1*x+a2*x^2+a3*x^3+ a4*x^4+a5*x^5)+(b0+b1*x+b2*x^2)
Reduced Chi-Sqr	0.03304
Adj. R-Square	0.99445
a0	-4915.96878±377.27164
a1	28.73493±27.73233
a2	-3.44994±0.46255
a3	0.08939±0.01049
a4	-8.31733E-4±1.07911E-4
a5	2.79449E-6±3.89508E-7
b0	16.15417±1.30235
b1	0.18096±0.09684
b2	-0.00242±0.00121

Figure S6. Virial fitting (lines) of the C_3H_6 adsorption isotherms (points) of Co-gallate measured at 273 and 298 K.

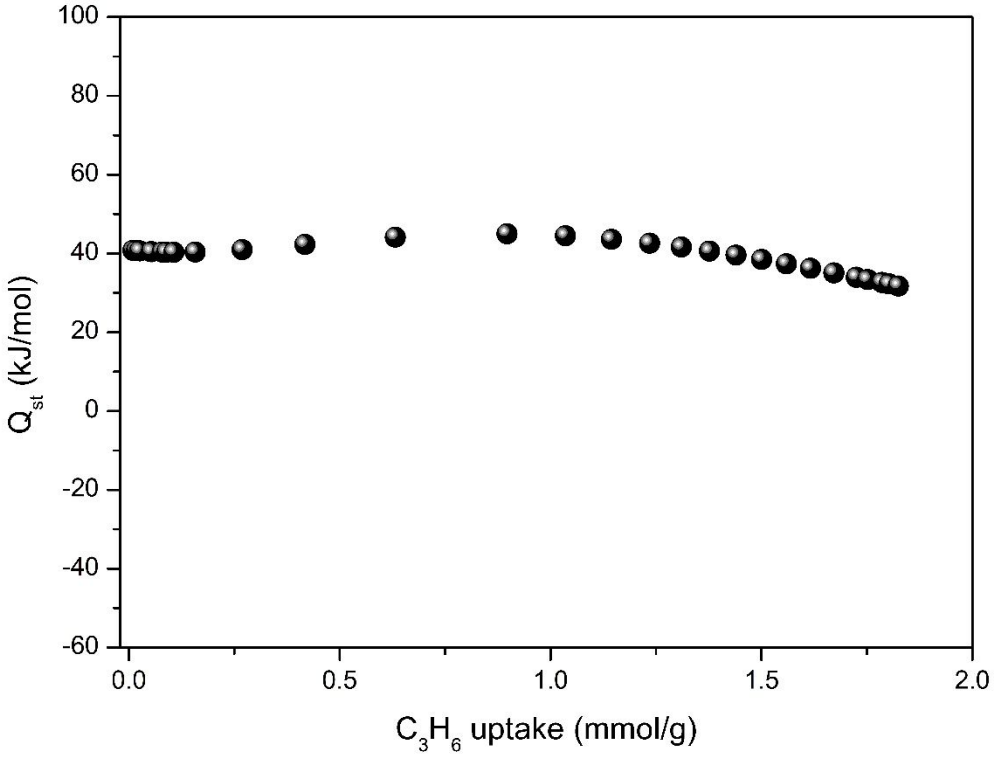

Figure S7. Enthalpies of adsorption for propylene.

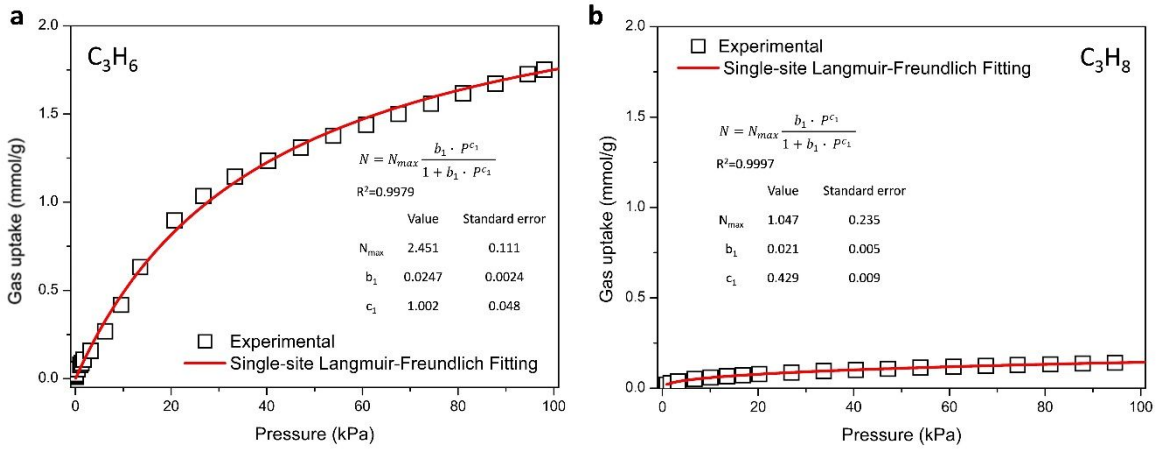

Figure S8. Langmuir-Freundlich fitting of the C_3H_6 (a) and C_3H_8 (b) sorption data at 298 K for Co-gallate.

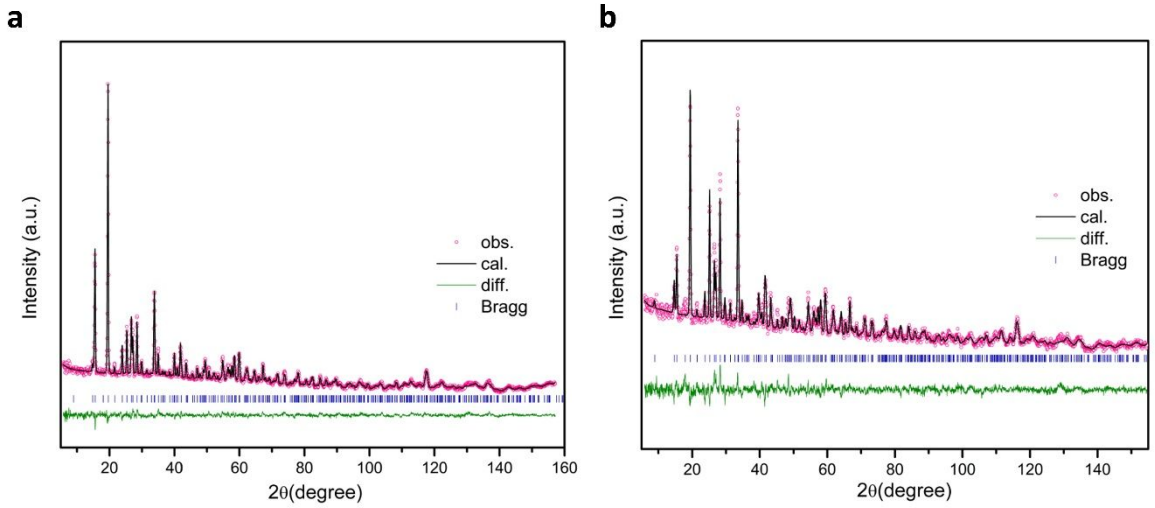

Figure S9. Rietveld refinements of the NPD data for a) bare Co-gallate and b) C_3D_6-loaded Co-gallate, both measured at 298 K. The ligand molecules and the C_3D_6 molecules were kept as rigid bodies during the refinement. Experimental (circles), calculated (line), and difference (line below observed and calculated) neutron powder diffraction profiles are shown. Vertical bars indicate the calculated positions of Bragg peaks.

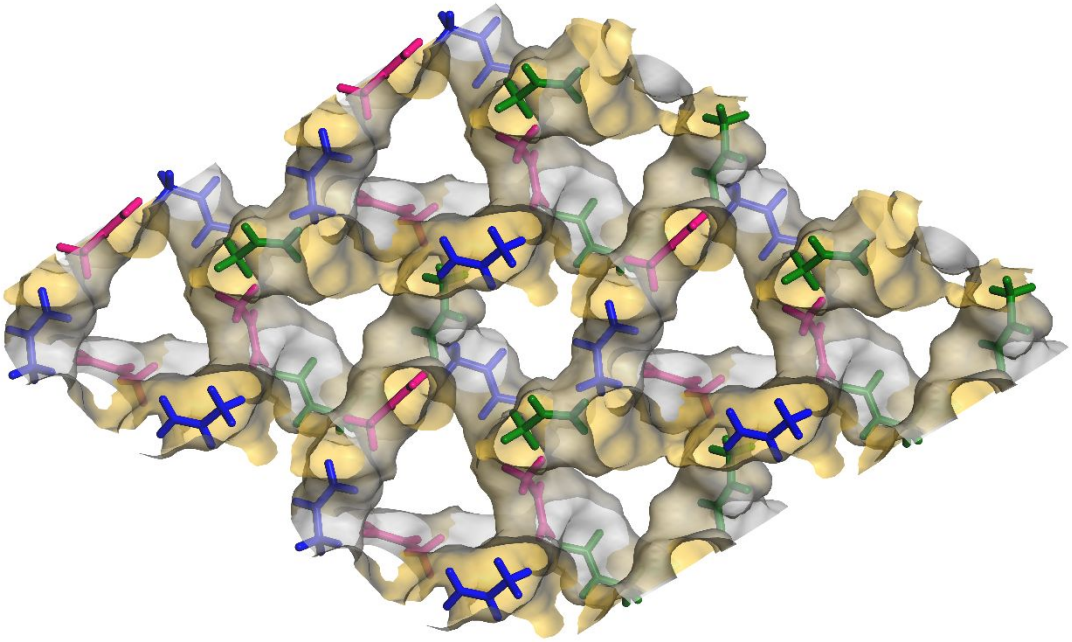

Figure S10. The packing diagram of the C_3D_6 absorbing structure. The preferential binding site for C_3D_6 (site I, site II and site III) are represented in blue, green and pink, respectively. The framework and the pore surface are shown in pale gold and yellow.

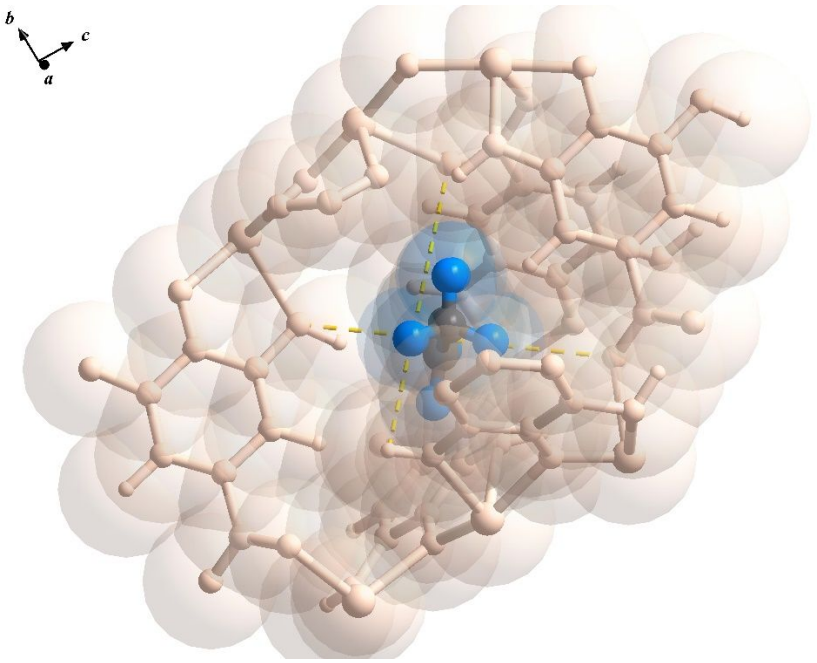

Figure S11. C_3D_6 configuration and pore dimensions of narrow intersection.

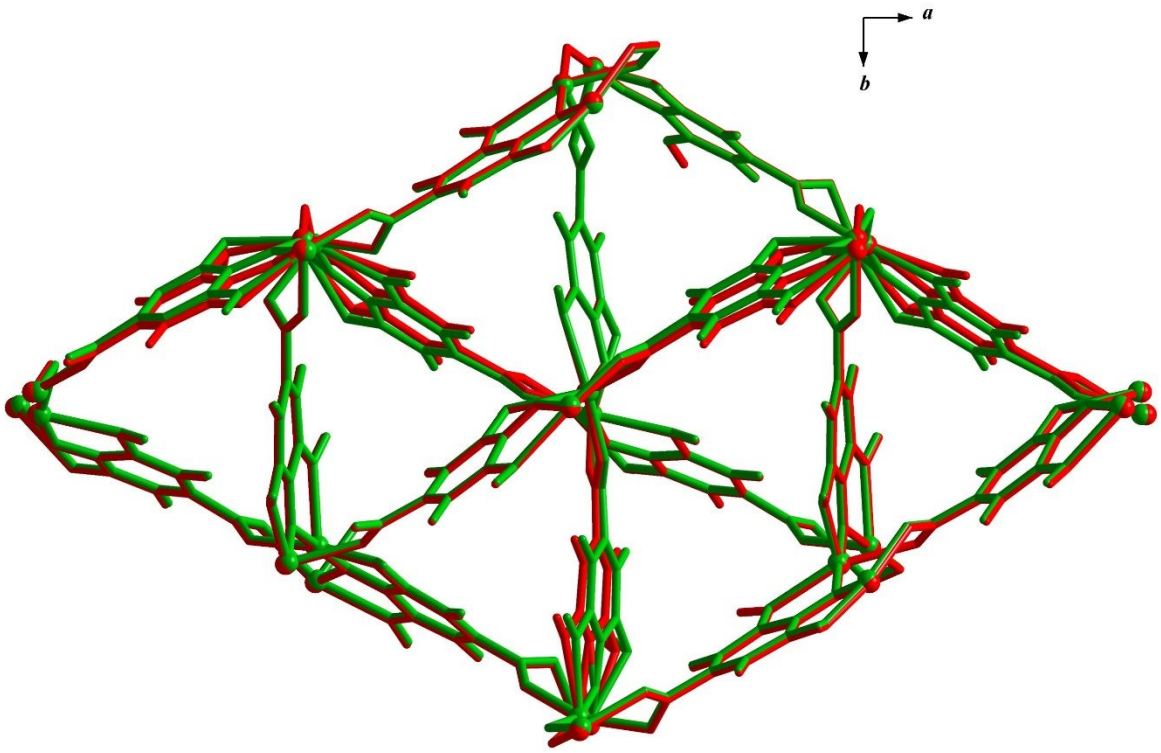

Figure S12. Negligible framework deformation in structural comparison of Co-gallate (green) and Co-gallate·0.38 C_3D_6 (red).

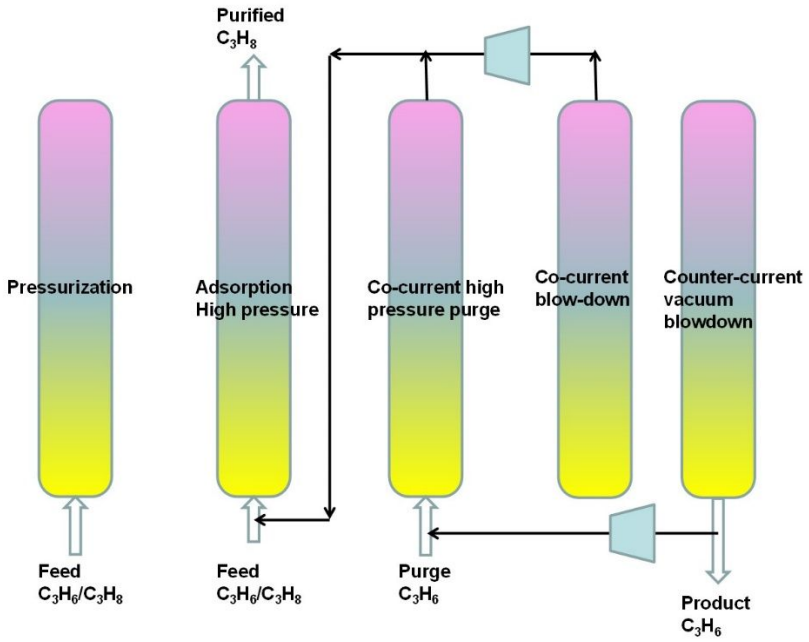

Figure S13. A pressure swing adsorption (PSA) system for C_3H_6/C_3H_8 separation.

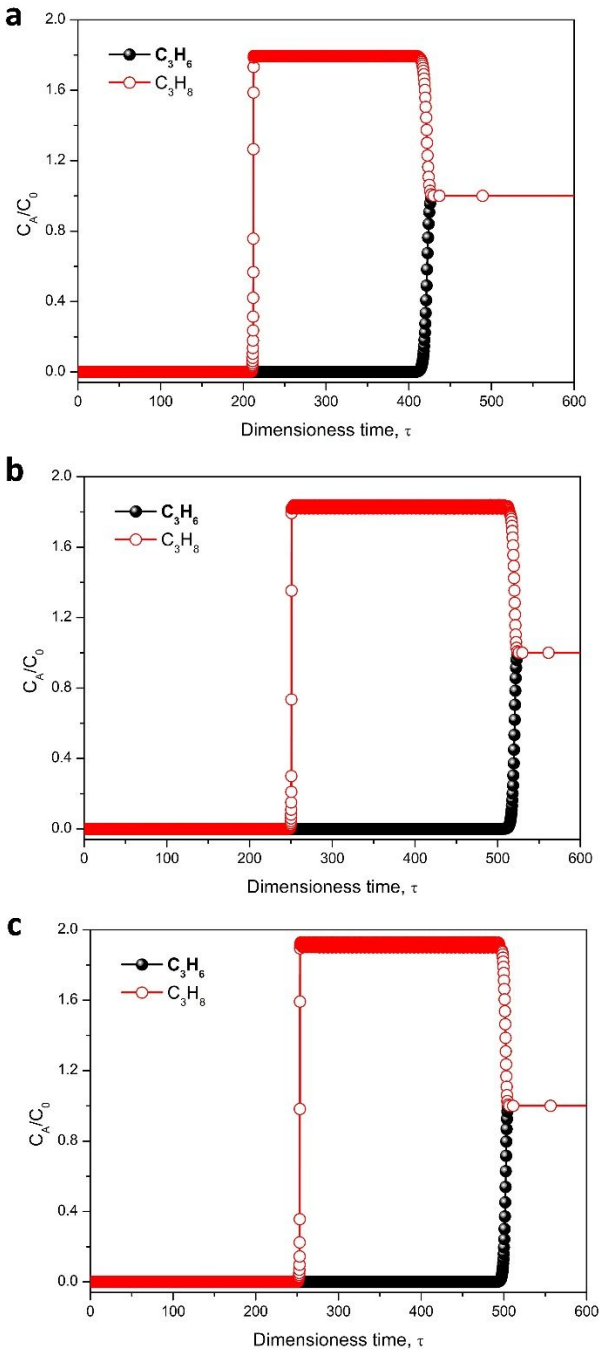

Figure S14. Transient breakthrough simulations of C_3H_6/ C_3H_8 (50:50, v/v) mixture on M_2(dobdc) at 298 K: a. Mg_2(dobdc); b. Co_2(dobdc); c. Fe_2(dobdc).

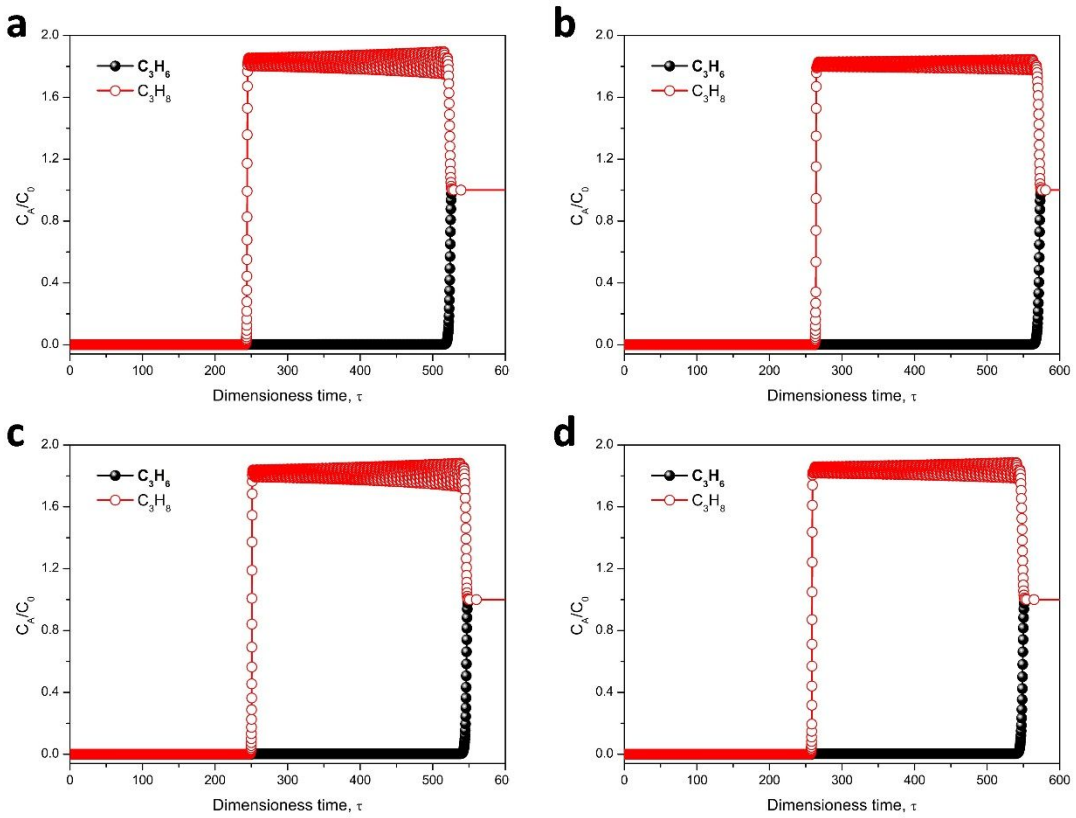

Figure S15. Transient breakthrough simulations of C_3H_6/ C_3H_8 (50:50, v/v) mixture on M_2(*m*-dobdc) at 298 K: a. Mn_2(*m*-dobdc); b. Co_2(*m*-dobdc); c. Fe_2(*m*-dobdc); d. Ni_2 (*m*-dobdc).

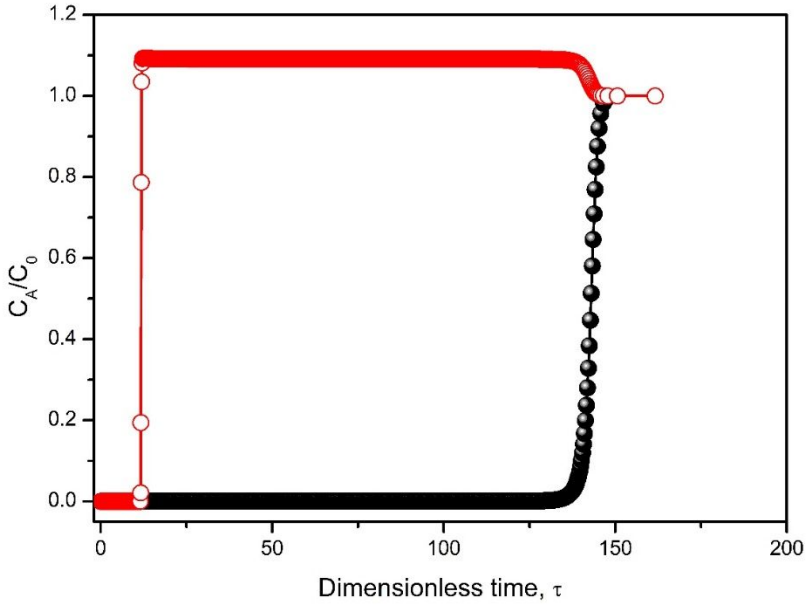

Figure S16. Transient breakthrough simulations of C_3H_6 (black)/ C_3H_8 (red) (50:50, v/v) mixture on Co-gallate at 298 K.

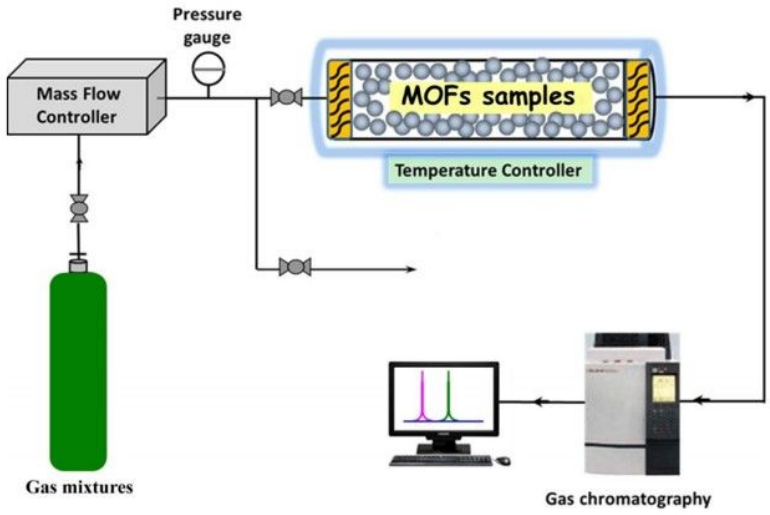

Figure S17. Schematic illustration of the apparatus for the breakthrough experiments.

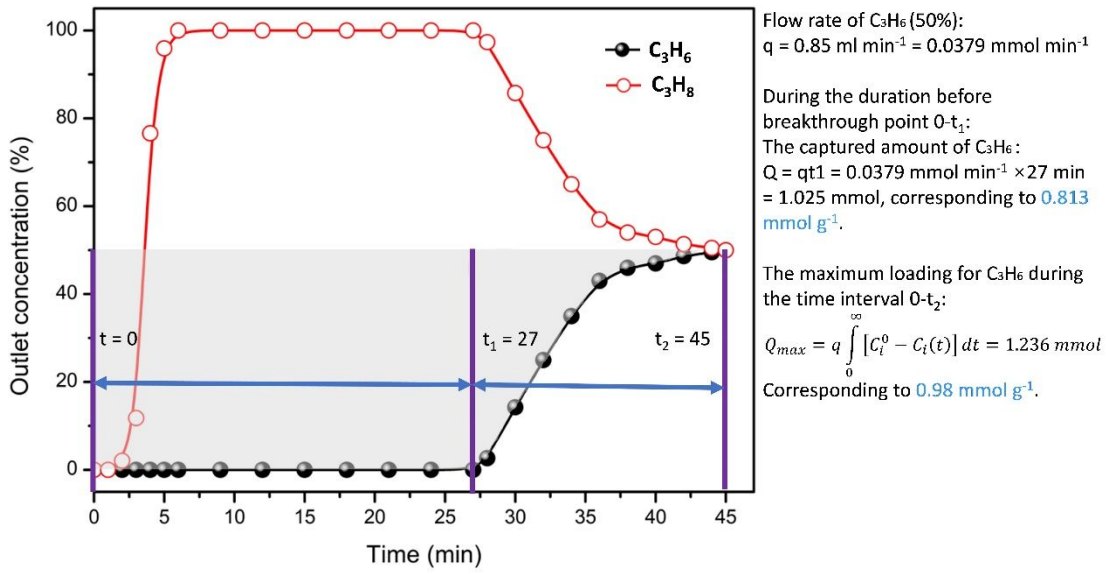

Figure S18. The calculation for captured amount of C_3H_6 during the breakthrough process in Co-gallate. During the duration before the breakthrough point (0-t_1), the captured C_3H_6 is 1.025 mmol, corresponding to 0.813 mmol g^{-1}. Considering the continuous C_3H_6 adsorption during the mass transfer zone (t_1-t_2), the integration of the grey area above the entire breakthrough curve gave the maximum loading of Co-gallate to be 1.236 mmol, corresponding to 36.4 cm^3/cm^3.

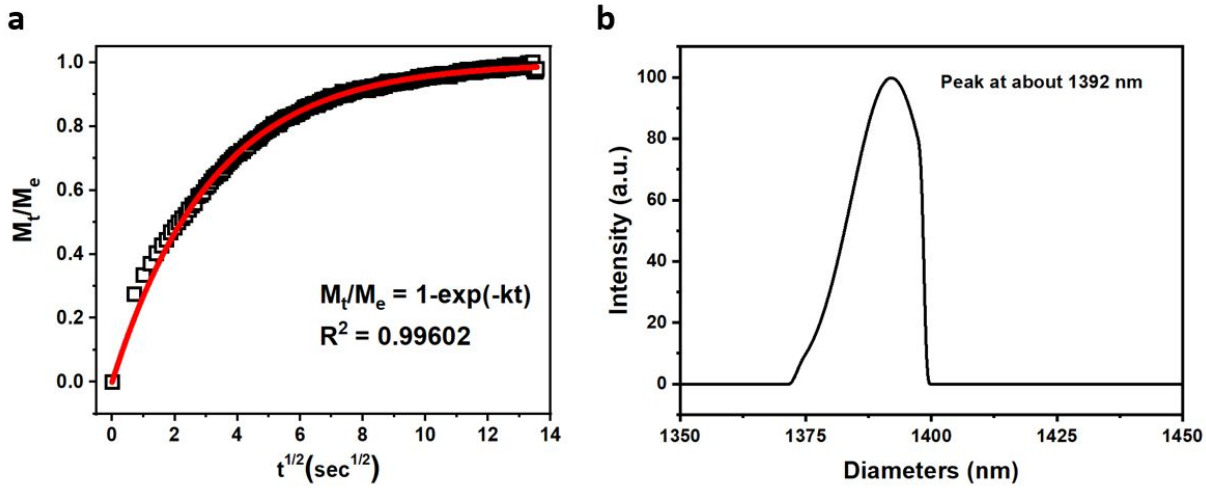

Figure S19. (a) Kinetic profile of Co-gallate for C_3H_6 adsorption at 298 K and equilibrium pressure of ~0.5 bar; (b) DLS size distribution of Co-gallate sample. The DLS measurements were performed with a NanoBrook (Brookhaven US) employing a 640 nm laser at 90° relative to the incident beam or at a backscattering angle of 173°. The diffusivity coefficient of propylene in Co-gallate has been calculated to be 4.05×10^{-10} cm^2/s, that is slightly lower than those of most microporous MOFs with kinetic separation mechanism (10^{-9}–10^{-8} cm^2/s, J. Phys. Chem. Lett. 2012, 3, 2130-2134. and *Reference 42*).

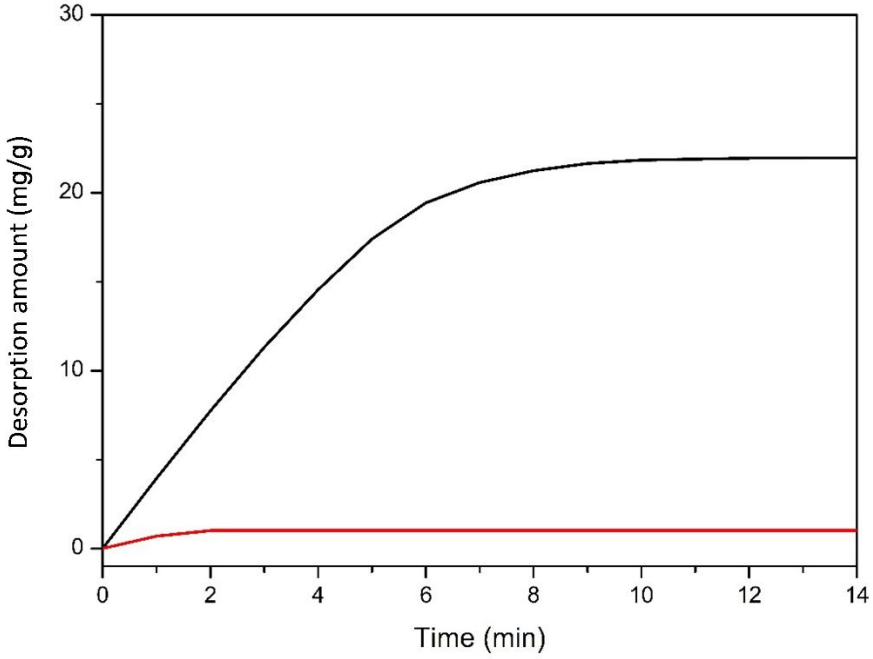

Figure S20. Desorption curve for an equimolar mixture of propane and propylene. Color scheme: black: propylene; red: propane.

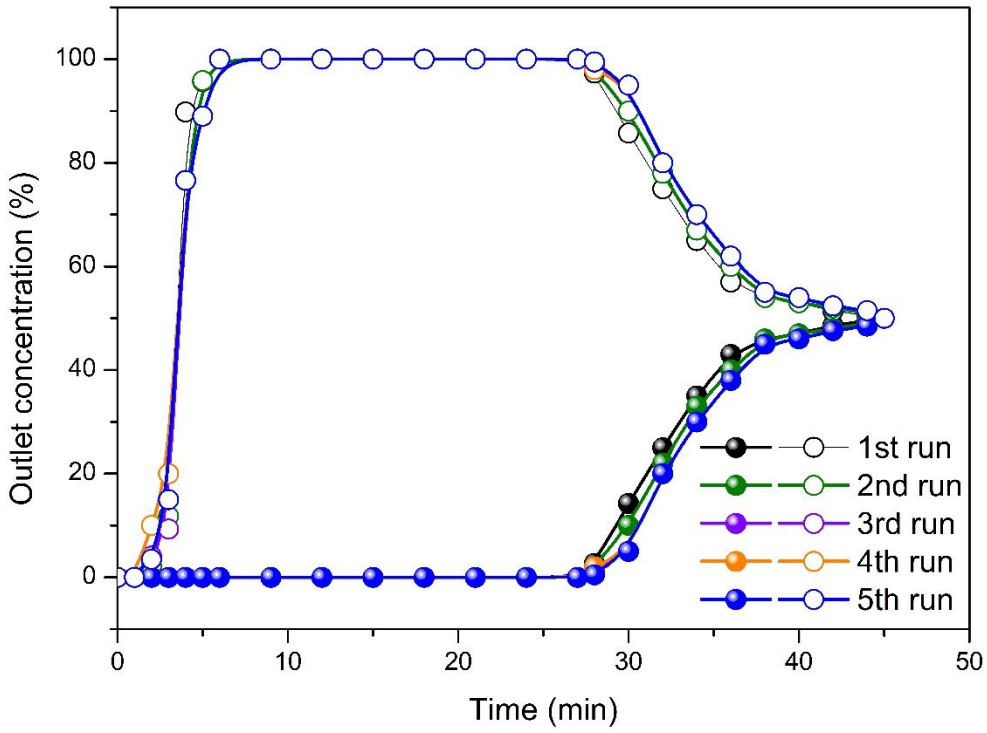

Figure S21. Multiple cycles of breakthrough curves for equimolar binary mixture of C3H6/C3H8 at 298 K and 1 bar. The breakthrough experiments were carried out in a packed column at a flow rate of 1.7 standard cubic centimeters per minute. Points are experimental data, and lines are drawn to guide the eye.

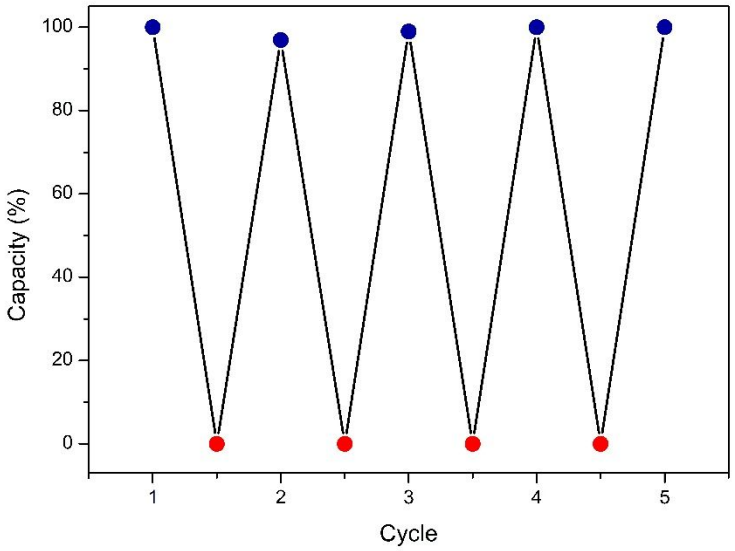

Figure S22. Cycling data for successive C_3H_6 adsorption and desorption. Adsorption capacities are expressed in terms of percentage of uptake relative to the first cycle. Adsorption (blue circles) was collected at 25 °C and 1 bar. Desorption (red circles) occurred by applying a helium gas flow (60 standard cubic centimeters per minute) for about 14 min at 298 K.

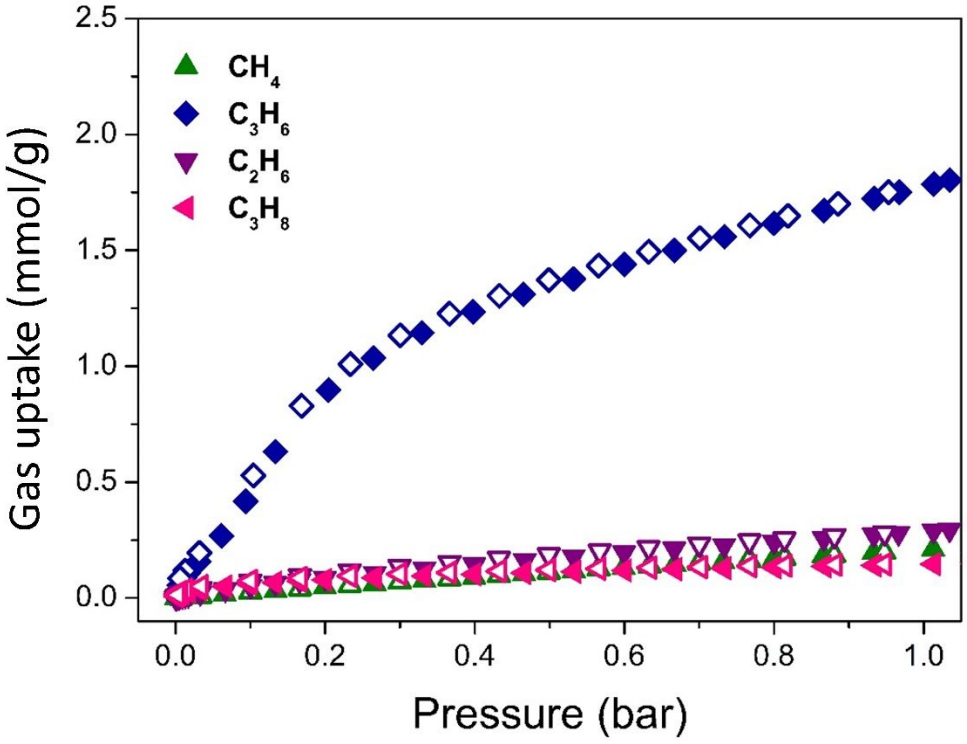

Figure S23. Single-component adsorption isotherms of CH_4 (green triangles), C_3H_6 (blue diamonds), C_2H_6 (purple diamonds), C_3H_8 (pink triangles) in Co-gallate MOF at 298 K.

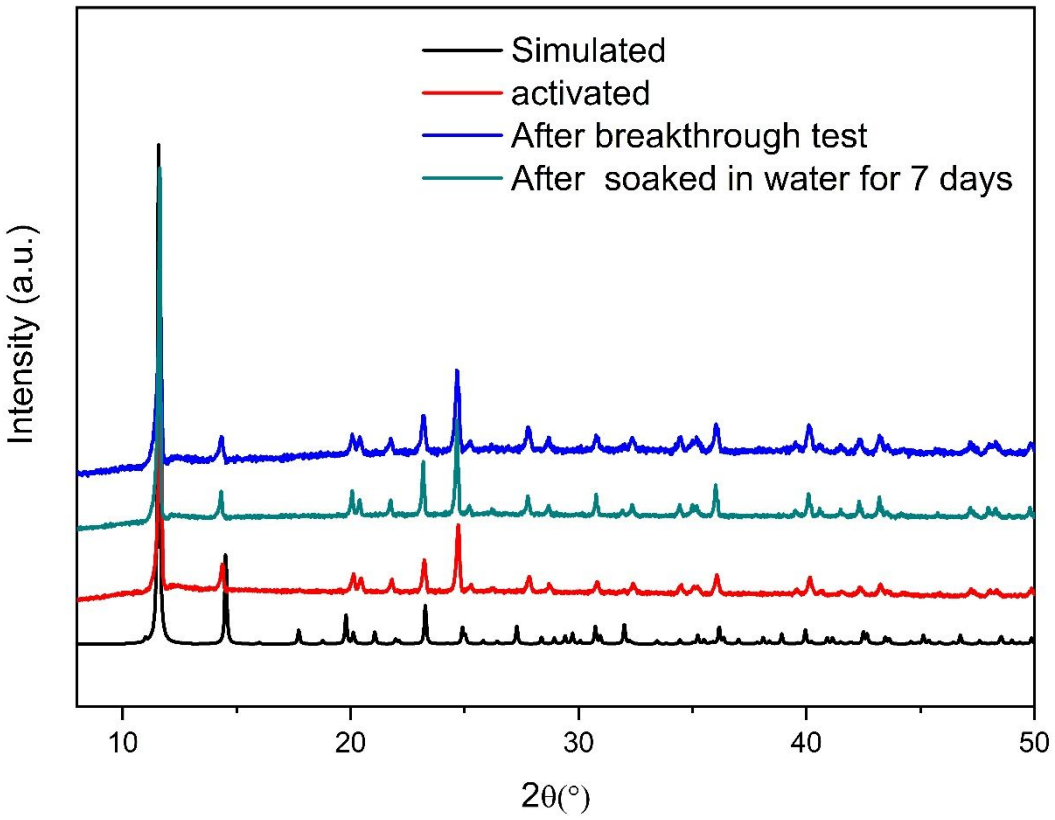

Figure S24. PXRD patterns of Co-gallate after breakthrough test and water stability tests.

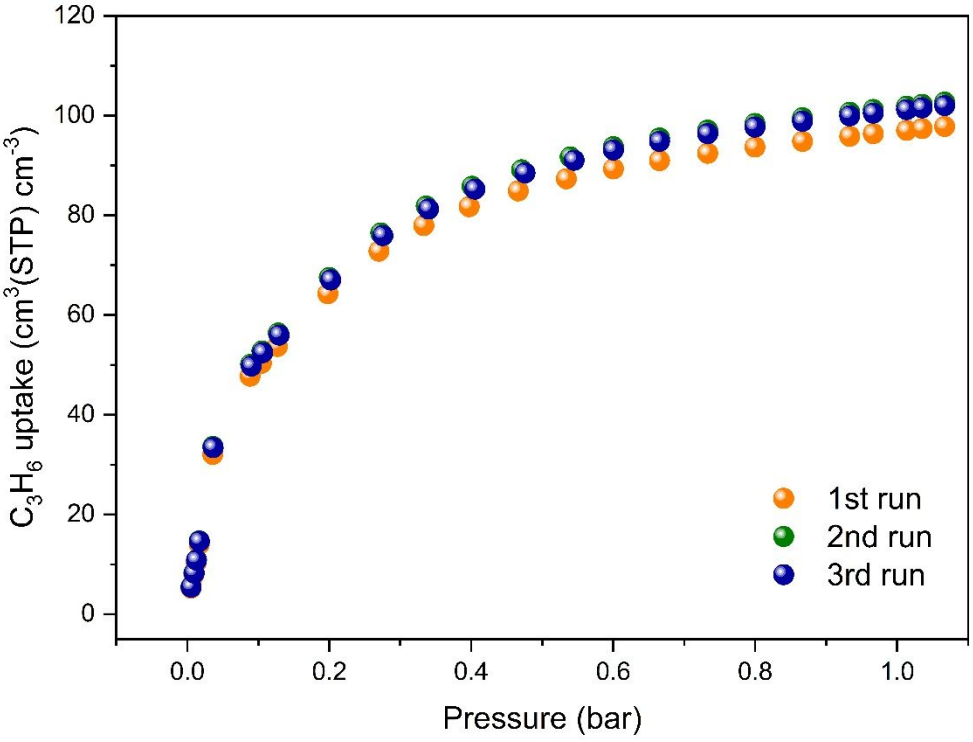

Figure S25. Multiple cycles of C_3H_6 adsorption isotherms for Co-gallate at 273 K after water immersion for one week.

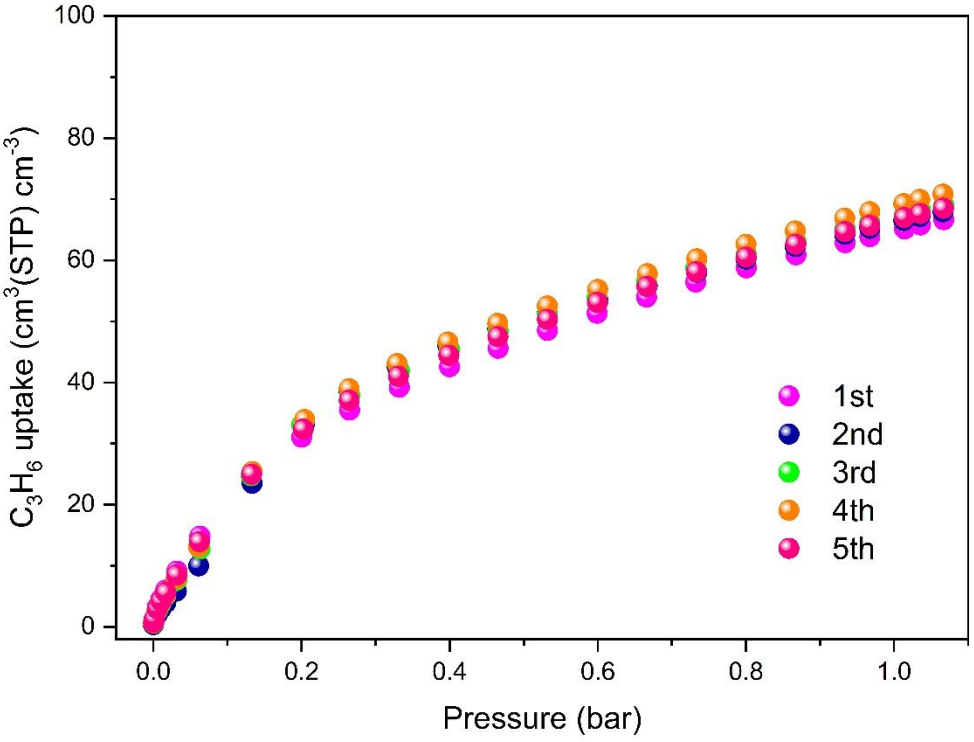

Figure S26. Multiple cycles of C_3H_6 adsorption isotherms for Co-gallate at 298 K and 0-1 bar after water immersion for one week.

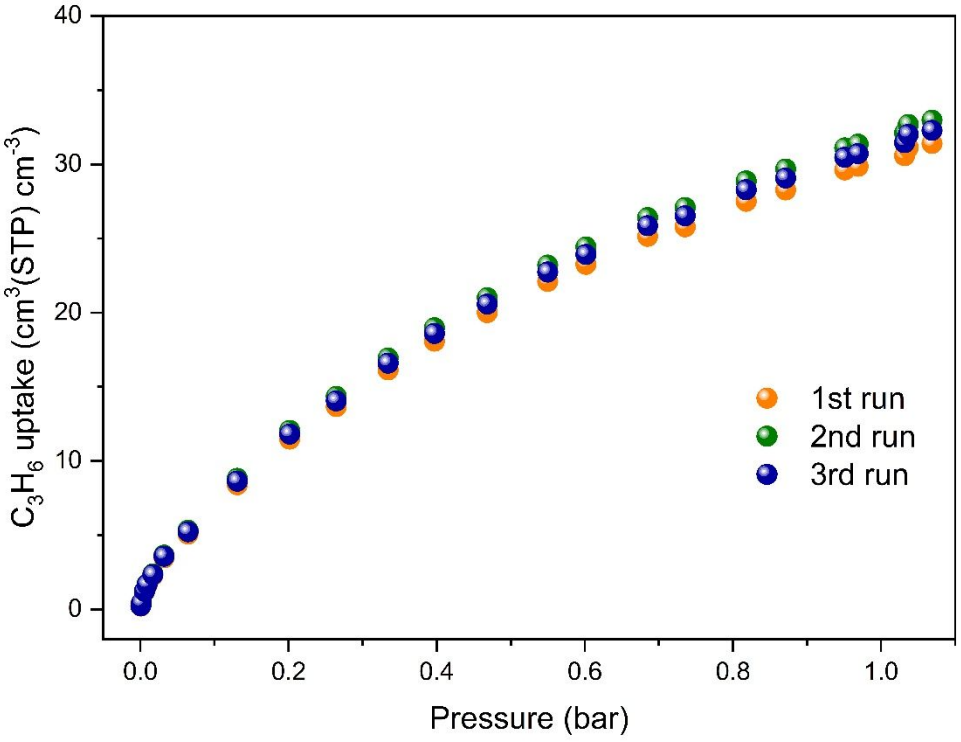

Figure S27. Multiple cycles of C_3H_6 sorption isotherms for Co-gallate at 313 K after water immersion for one week.

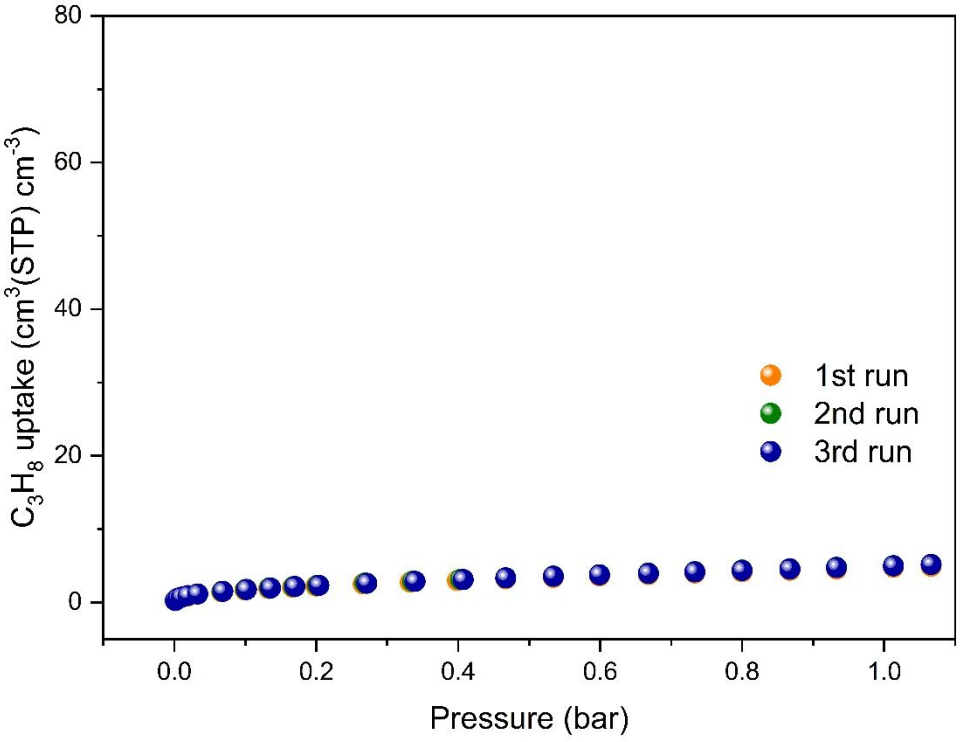

Figure S28. Multiple cycles of C_3H_8 adsorption isotherms for Co-gallate at 273 K after water immersion for one week.

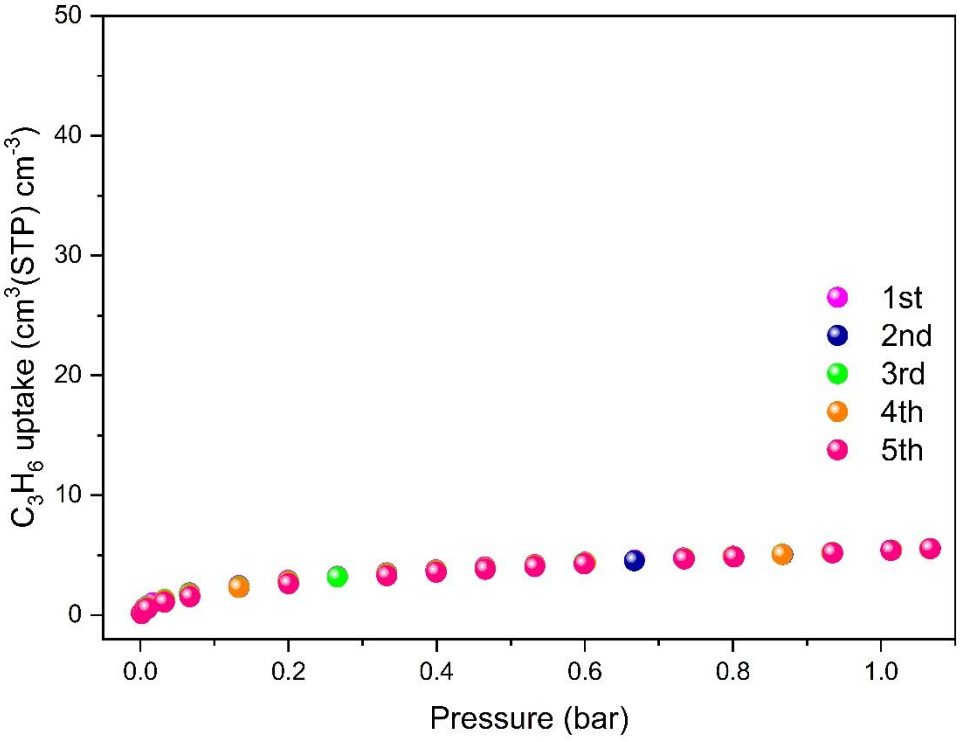

Figure S29. Multiple cycles of C_3H_8 adsorption isotherms for Co-gallate at 298 K after water immersion for one week.

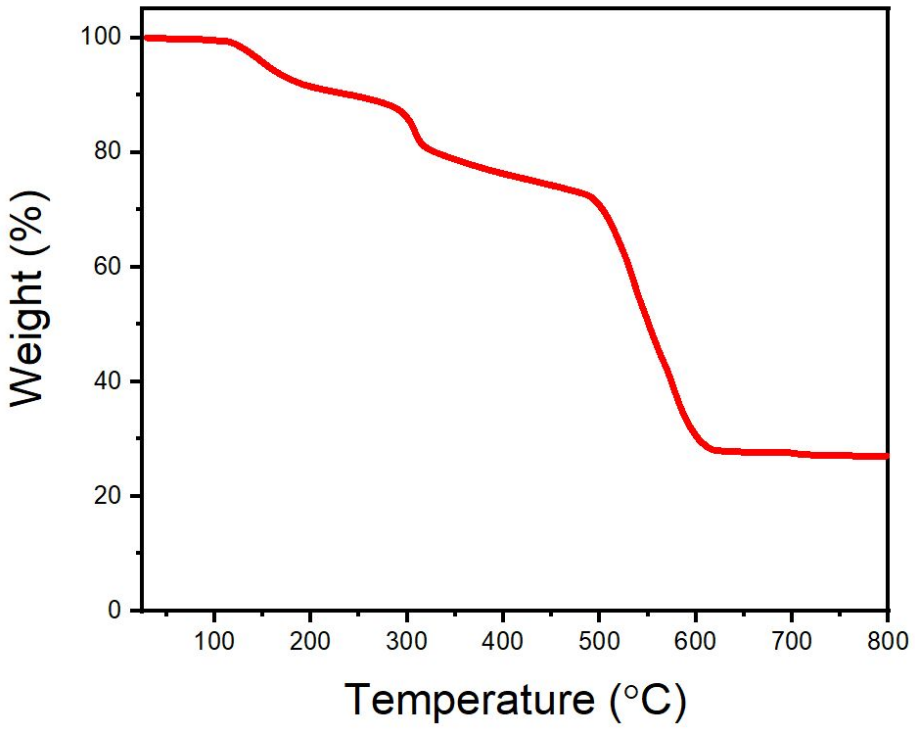

Figure S30. TGA curves for Co-gallate.

Additional Tables

Table S1. Comparison of physical parameters of C_3H_6 and C_3H_8.[4]

	Molecular weight (g mol^{-1})	Kinetic diameter (Å)	Boiling point (K)	Polarizability (10^{-25} cm^3)	Dipole moment (10^{-18} esu cm)
C_3H_6	42.08	4.7	225.5	62.6	0.366
C_3H_8	44.10	5.1	231.1	62.9-63.7	0.084

Table S2. Crystal data and structure refinements of Co-gallate with C_3D_6 inclusions.

Complex	Co-gallate	Co-gallate·C_3D_6
Formula	$C_{21}H_{12}Co_3O_{15}$	$C_{24.41}H_{12}D_{6.83}Co_3O_{15}$
F.W.	681.10	735.82
Temperature (K)	298	298
Crystal system	Trigonal	Trigonal
Space group	P31	P31
a	15.27	15.38
b	15.27	15.38
c	10.11	10.19
α	90	90
β	90	90
γ	120	120
Cell volume (Å^3)	2041.17	2085.7
Z	3	3
D_{calc} (g/cm^3)	1.662	1.758
μ (1/mm)	0.000	0.000
F(000)	567.8	1098.75
R_p	0.0146	0.0194
wR_p	0.0177	0.0236

Table S3. Summary of the gas uptakes, selectivities and Qst for C_3H_6, C_3H_8 in various porous materials.

Materials	*T* (K)	*P* (bar)	Density (g cm^{-3})	C_3H_6 uptake (cm^3cm^{-3})	C_3H_8 uptake (cm^3 cm^{-3})	IAST selectivity @1 bar	Q_{st} of C_3H_6 (kJ mol^{-1})
Ni_2(dobdc)[5]	298	1	1.206	131	107	12	--
Co_2(dobdc)[29]	298	1	1.169	192	141	46	--
Mg_2(dobdc)[27]	318	1	0.909	171	144	7.5	--
Fe_2(dobdc) [27]	318	1	1.126	174	153	15	--
$Cr_3(btc)_2$[27]	308	1	0.83	180	160	3.0	--
$Cu_3(btc)_2$[27]	318	1.5	0.879	124	98.4	6.1	--
13X zeolite[27]	318	1	1.47	69.1	52.7	8.2	--
Mn_2(dobdc)[40]	318	1	1.133	175	120	25	54.1
Mn_2(*m*-dobdc)[41]	298	1	1.16	188	154	43	67.4
Fe_2(*m*-dobdc) [41]	298	1	1.16	190	154	60	73.0
Co_2(*m*-dobdc) [41]	298	1	1.183	200	160	38	53.1
Ni_2(*m*-dobdc) [41]	298	1	1.200	197	163	35	55.1
MAF-23[42]	298	1	1.428	62.4	61.4	3.2	60.2
MAF-23-O[42]	298	1	1.459	44.1	32.7	8.8	78.0
KAUST-7[37]	298	1	1.802	56.8	--	--	57.4
Y-abtc[38]	298	1	1.457	63.5	--	--	50.0
Co-gallate	**298**	**1**	**1.662**	**66.6**	**5.2**	**333**[a]	**41.0**

[a] IAST selectivity value is only for the qualitative comparison purpose.

Table S4. Comparison of dynamic selectivity and purity of C_3H_6 calculated from transient breakthrough simulation.

MOF	Dynamic selectivity	C_3H_6 Purity (100 %)
Mn_2(*m*-dobdc)	40.1	97.6
Co_2(*m*-dobdc)	40.3	97.6
Fe_2(*m*-dobdc)	55.7	98.2
Ni_2(*m*-dobdc)	34.3	97.2
Co_2(dobdc)	18.7	94.9
Fe_2(dobdc)	18.9	95.0
Mg_2(dobdc)	9.2	90.2
Co-gallate	47533	99.998

*The dynamic selectivity and purity are calculated based on the integration proportion of transient breakthrough simulations curves.

Table S5. Host-guest interactions within the structure of Co-gallate loaded with C_3D_6.

Site I				Site II				Site III			
	Y···D (Å)	X-D···Y (Å)	θ (°)		Y···D (Å)	X-D···Y (Å)	θ (°)		Y···D (Å)	X-D···Y (Å)	θ (°)
C111-D115···O22	2.49(5)	3.55(5)	162	C123-D127 ···O21	2.97(2)	3.84(2)	137	C132-D136 ···O21	1.99(3)	2.72(3)	121
C111-D115···O29	3.18(4)	3.67(5)	109	C122-D126···O2	2.01(2)	2.77(2)	124	C131-D139···O21	2.63(2)	3.11(3)	106
C112-D116···O44	1.92(4)	2.53(4)	112	C121-D125···O17	2.71(2)	3.73(2)	156	C131-D135···O29	3.20(3)	4.03(3)	133
C112-D116···O33	1.97(4)	2.67(5)	138	C121-D124···O11	2.51(2)	2.85(3)	97				
C113-D117··· $\pi_{aromatic}$	2.61(4)	3.43(4)	131	C123-D129··· $\pi_{aromatic}$	2.07(1)	2.94(1)	133	C131-D135··· $\pi_{aromatic}$	2.18(3)	3.17(3)	150
C123-D119··· $\pi_{aromatic}$	3.15(5)	3.60(5)	105	C123-D129···$\pi_{aromatic}$	2.21(2)	2.79(2)	110	C133-D137··· $\pi_{aromatic}$	2.77(2)	3.05(2)	94
C111-D114··· $\pi_{aromatic}$	2.91(4)	3.68(4)	128								
O11-H15 ···$\pi_{=}$	2.28(2)	3.18(2)	150	O43-H47 ···$\pi_{=}$	2.47(2)	3.29(2)	141				
O2-H10 ···$\pi_{=}$	2.87(1)	3.69(1)	142								

References

1. Feller, R. K.; Cheetham, A. K., Fe(III), Mn(II), Co(II), and Ni(II) 3,4,5-trihydroxybenzoate (gallate) dihydrates; a new family of hybrid framework materials. *Solid State Sci.* **2006,** *8* (9), 1121-1125.

2. Krishna, R., The Maxwell–Stefan description of mixture diffusion in nanoporous crystalline materials. *Micropor. Mesopor. Mat.* **2014,** *185*, 30-50.

3. Webster, C. E.; Drago, R. S.; Zerner, M. C., Molecular dimensions for adsorptives. *J. Am. Chem. Soc.* **1998**, 120(22), 5509-5516.

4. Li, J.-R.; Kuppler, R. J.; Zhou, H.-C., Selective gas adsorption and separation in metal-organic frameworks. *Chem. Soc. Rev.* **2009**, 38(5), 1477-1504.

5. Chen, D.-L.; Shang, H.; Zhu, W.; Krishna, R., Reprint of: Transient breakthroughs of CO_2 /CH_4 and C_3H_6/C_3H_8 mixtures in fixed beds packed with Ni-MOF-74. *Chem. Eng. Sci.* **2015**, 124, 109-117.